Master's thesis

Performance measurement of Hermite-based multi-carrier communication

Author:
Mark de Ruiter (s1119583)

Committee:
Prof. Dr. Ir. G.J.M. Smit
Dr. Ir. A.B.J. Kokkeler
Dr. Ir. A. Meijerink
C.W. Korevaar MSc

Computer Architecture for Embedded Systems (CAES) chair
University of Twente

August 20, 2014

Abstract

Because today's world exhibits an increasing demand for wireless communication, available bandwidth in the electro-magnetic spectrum is becoming scarce. Therefore, it is important to use it more efficiently. The widely applied transmission scheme orthogonal frequency-division multiplexing (OFDM) has shortcomings when high efficiency is required in a multi-user setting. This scheme employs an orthogonal set of truncated sinusoids as the basis of the transmission signal, giving spectral sidelobes that interfere with other users. Tight synchronization between the users is required to avoid mutual interference when the cost of increased frequency spacing, i.e. lower spectral efficiency, is undesirable.

Conventional approaches of this problem leave the sinusoidal basis signals intact and thereby only combat the symptoms. As an alternative solution, it was suggested to change from sinusoids to a completely different set of basis signals for transmission: Hermite functions. These functions are well-localized in time-frequency according to their second-order moments and therefore theoretically cause minimal interference to other users when employed as basis signals. The first function of the set is a Gaussian function, which is known to be the optimally time-frequency concentrated function.

The current work presents the results of an investigation in the applicability of Hermite functions as a set of basis signals for wireless communication. Despite being well-localized in time-frequency regarding the second-order moments, Hermite functions exhibit exponential tails that extend infinitely both in time and in frequency. The resulting overlap between different symbols causes inter-symbol interference (ISI), that increases with symbol density. Spectral efficiency depends on the density of symbols in the time-frequency plane, the number of basis signals and the employed modulation scheme. Analyses, simulations and measurements in this thesis are focussed on the question what the maximum achievable spectral efficiency of a Hermite system is, when the bit-error ratio (BER) resulting from ISI is constrained. Because a rigorous mathematical analysis of the inherent interference tends to burst with complexity, the simulations and measurements attain a prominent role in the anwer to this question.

When spectral efficiency is maximized, there is intuitively little tolerance on symbol positions in time-frequency. Because the unsynchronized multi-user situation is the intended application of the Hermite system, questions about its robustness against missynchronization are relevant. The missynchronization tolerance depends on the characteristics of the relation between the synchronization error and the BER. This relation is inspected by means of simulations and compared to that of a traditional OFDM system.

A major goal of the current work is verification of theoretical performance by the actual transmission of data using physical transceivers. To accomplish this goal, an experimental setup consisting of globally available hardware is made. The real-world transmissions of data with Hermite functions lead to results that support theoretical performance figures.

It is seen that spectral leakage of a Hermite-based system is low when compared to OFDM. According to the results of the current work, the Hermite basis gives the advantage of well-controllable robustness against missynchronization between different users, while achieving close-to-optimal spectral efficiency. Therefore, the Hermite functions give hope of a future with improved utilization of the electro-magnetic spectrum.

Preface

About one and a half years it took: the work for this thesis. Not full-time, I must admit. Several developments and events during this period prevented a perfectly smooth process. However, here I am, finally filling this last "white space". Part of me is glad that it's almost done, another part looks back on my time in Twente and feels sad that this phase is ending.

I would like to thank all the people who were somehow involved in the process. First of all, Wim Korevaar for coming up with the idea of Hermite-based communication and for his seemingly infinite enthousiasm. I think you are the first person I met, who, upon receiving a visually-supported explanation of a certain phenomenon, replied with something like "I don't get it yet, I need to see equations first." Some other time I heard someone sigh of despondency, because he had to read *and understand* a paper you wrote, which seemed packed with mathematical acrobatics. I also want to thank André Kokkeler, for joining forces with Wim to be my daily supervisors and provide me with feedback. Your calm and patience was very valuable. I want to thank you both for all your support.

Of course, I also want to thank Arjan Meijerink and Gerard Smit for being in my graduation committee. Furthermore, I thank everyone of the CAES group for providing a pleasant work environment with the occasional necessary relaxing moments. I enjoyed the lunch walks very much and the coffee breaks were often a very welcome relief from uncomfortably complex thinking. In particular I want to thank Bert Molenkamp and Koen Blom for my initial encounters with CAES and supervising the individual assignment for my premaster program.

Another thank you goes to my neighbor Harrie Knoef, because he was willing to review parts of my thesis. Finally, I thank my family: my parents Dirk & Mieke de Ruiter and my brother Siebert for their support and encouragements and my uncle and aunt Cees & Jellie de Ruiter for opening up their home for me to live the past couple of years.

Mark de Ruiter

Contents

Chapter 1

Introduction

Today's world is all about connecting and communicating. Telephony and the internet provide communications between an increasing number of people all over the world. Furthermore, wireless computer networks have become common facilities in homes, providing connections between laptops, smartphones, television sets and printers.

Although devices, such as a door bell and its push button, were traditionally connected by wires, there seems to be a global trend to use wireless connections instead. Furthermore, people's increased mobility is a driving force for wireless communication. In less-developed countries, the phase of rolling-out wired telecommunication networks is even skipped and focus is going straight to connections by radio waves [19], because wireless infrastructure has become relatively inexpensive.

In general, establishing and maintaining a reliable wireless connection with large capacity is technically much more challenging than a wired equivalent. But the shift from wired to wireless connections does not mean that people have lowered their standards with regards to capacity and reliability. On the contrary: demands for capacity have increased, e.g. because people want to view high-quality video on their mobile devices, and as more aspects of our lives rely on the connections' presence, reliability becomes ever more important.

One of the problems accompanying these developments, is that the available electromagnetic spectrum is becoming scarce [40]. Every single transmitter occupies a piece of spectrum for some time. During this time, other transmitters can not use the same piece without causing interference. Luckily, the geographical range covered by a transmitter is limited, allowing the reuse of spectrum in different areas. But the required distance to cover is very dependent on the specific application: it can be a few centimeters or even thousands of kilometers.

To maintain interference-free operation of certain connections, national and international regulatory bodies (e.g. the Federal Communications Commission (FCC) in the US) allocate bands in the spectrum for particular services or licensees, such as television broadcast and cellular network providers. Because the cost of spectrum licenses increases with bandwidth, it is beneficial for licensees to minimize the occupied bandwidth per transmitter. The allocations are usually fixed for a prolonged period and cover a large geographical area [2]. This rigid allocation of spectrum contributes to inefficient use of the spectrum, because many allocated bands are not continuously in use by the licensee. Currently, only 2% – 20% of the usable spectrum is active at an arbitrary time and place [37].

The problem of scarcity and inefficient use of the electromagnetic spectrum has stimulated researchers to investigate what is called cognitive radio (CR). By employing dynamic spectrum access (DSA), a CR can use locally and temporarily available bands, often called white spaces or spectrum holes. Although these bands may be allocated to a primary user (PU), the CR, as a secondary user (SU), is allowed to use them, but under certain conditions. An important condition is that the SU should not interfere with any PU's system. As a consequence, the SU's occupied bandwidth must fit in the spectrum hole and thus out-of-band emissions must be extremely low.

Minimization of required bandwidth is one of the stimuli for the subject of this thesis.

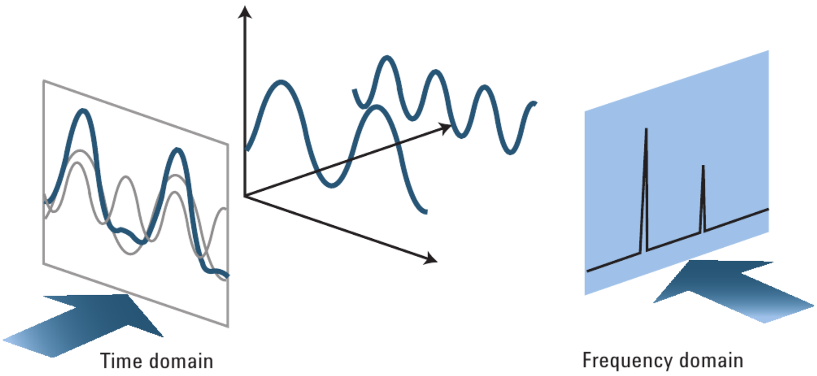

Figure 1.1: *Relationship between time domain and frequency domain. The thick curve in the left "window" shows the time-domain representation of a function. The function can be thought of as the sum of the two sinusoids. The graph on the right visualizes the frequency-domain representation. (image from [1])*

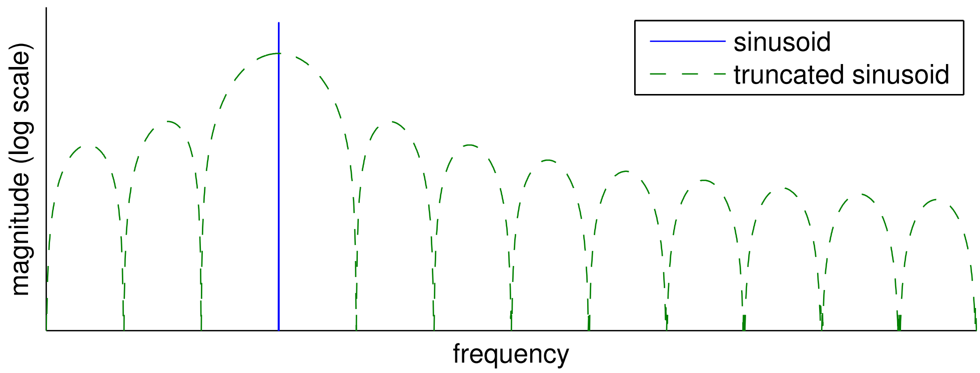

Figure 1.2: *Frequency magnitude representations of a sine and its truncated version*

1.1 Periodicity, sinusoids and Fourier

Earth's nature knows many periodic phenomena: day and night alternate, causing animals to sleep and wake; four seasons appear in a fixed order each year, changing the colors of trees and plants accordingly; and so on. These things are often related to the behavior of celestial bodies, that show rotations and travel in elliptical orbits.

In mathematics, sinusoids[1] are well-known periodic functions. They are at the heart of theories developed by Joseph Fourier (1768-1830) [7]. Fourier stated that an arbitrary periodic function can be represented by a series of sinusoids, whose frequencies are multiples of the original function's frequency. This representation is called a Fourier series. More generally, the Fourier *transform* allows a similar representation of both periodic and non-periodic functions.

The weights and frequencies of all sinusoids in the Fourier representation give information about the spectral content of the function. It is said that the Fourier transform gives the frequency-domain representation of the original (time-domain) function. Figure 1.1 illustrates the relation between time domain and frequency domain.

Natural phenomena are often called periodic when they show periodic behavior for some finite time. Sinusoids are periodic functions in a strict sense: their periodic behavior never ends. The frequency-domain representation of a strictly periodic function exhibits (infinitely) narrow peaks at particular frequencies. For example, a sine of a certain frequency causes a peak at that same frequency in the frequency domain. However, a truncated version of the same sine is no longer strictly periodic and exhibits a sinc-shaped curve around this frequency. See Figure 1.2. The function that was

[1]In this thesis, the general term "sinusoids" includes sine and cosine functions, as well as complex exponentials.

obtained by truncation is sometimes regarded as having a certain center frequency, corresponding to the frequency of the original sine.

In electrical engineering, the values over time of particular voltages or currents within a circuit are often called signals. Signals can mathematically be represented by functions in theoretical treatises, allowing frequency-domain analysis of the signals by means of the Fourier transform.

1.2 Wireless data transfer

A field of electrical engineering in which frequency-domain analysis plays a prominent role, is that of (wireless) communications systems. Radio systems exploit the properties of radio frequency (RF) signals, that enable them to travel from one place (antenna) to another without needing a visible medium, such as a wire.

Transferring a binary digit by wire can be realized by placing, for some time interval, a voltage with one of two polarities on a pair of wires. Each polarity corresponds to one of the two possible bit values. At the other end of the wires, the receiver measures the voltage polarity to find the bit value. Obviously, multiple bits can be transferred by repeating this for subsequent time intervals. The transmitted signal consists of a series of (rectangular) voltage pulses and its frequency-domain representation shows the shape of a sinc-function, centered at 0 Hz.

For wireless data transfer, the pulse signal is used to modulate a carrier signal, causing the latter to “carry” the data. Wireless propagation is possible, because the carrier signal is a sinusoid at RF. The frequency-domain representation of the result shows the same sinc-shape of the pulse signal, but centered at the carrier frequency. To demodulate the signal, the receiver uses a similar carrier signal at the same frequency. Ideally, the original pulse signal is the result of the demodulation.

When frequency-division multiplexing (FDM) is employed, multiple, individually modulated carriers of different frequencies are summed, either in the electronic circuitry or when travelling through the medium. In the latter case, each carrier comes from a different transmitter, hence frequency-division multiple access (FDMA) is employed. When multiple carriers come from a single transmitter, the scheme is referred to as multi-carrier modulation.

Because the sinc-shape spreads widely in the frequency domain, the different carriers can cause interference to each other’s signals. The result is that bits are misinterpreted at the receiver, impairing data integrity. A traditional solution consists of choosing the carrier frequencies far apart, but this means that less carriers can be placed in a certain bandwidth, i.e. spectral efficiency is lower. With the nowadays-popular multi-carrier scheme OFDM, a set of orthogonal sinusoids is used as the subcarriers of a transmitter. Because these sinusoids are spaced very closely in frequency, spectral efficiency is high. Orthogonality of the carriers ensures that no inter-carrier interference (ICI) occurs. OFDM is employed in many contemporary wired and wireless communication systems, of which Digital Subscriber Line (DSL) and wireless LAN (WLAN) are probably best known. A corresponding scheme for multiple transmitters is referred to as orthogonal frequency division multiple access (OFDMA).

However, OFDM is known to suffer from ICI when transmitter and receiver carrier frequencies are not synchronized. Furthermore, timing missynchronization causes ISI. For OFDMA, missynchronization between different users leads to even more interference, which is sometimes referred to as multiple-access interference (MAI) [34]. Missynchronization is caused notably by mismatch of individual devices’ local oscillators (LOs), which is unavoidable because of differences in electronic components and environments. Other causes are wireless-channel effects, such as Doppler-shifts.

1.3 Battling spectral inefficiency in a multi-user situation

Spectrum scarcity, in combination with the shortcomings of existing communication schemes regarding spectral leakage and synchronization robustness in multi-user situations, calls for drastic improvements in the way wireless communication is performed.

One possible solution is examined by Wim Korevaar in [23]. He proposed proposed to switch from sinusoid-based signals to signals based on Hermite functions, in order to reduce the spectral leakage associated with the truncated sinusoids. These functions, illustrated in Figure 1.3, are non-periodic and their energy is well-localized in both the time domain and the frequency domain. In fact, the functions exhibit the same curve shape in both domains. Furthermore, their spectral magnitude

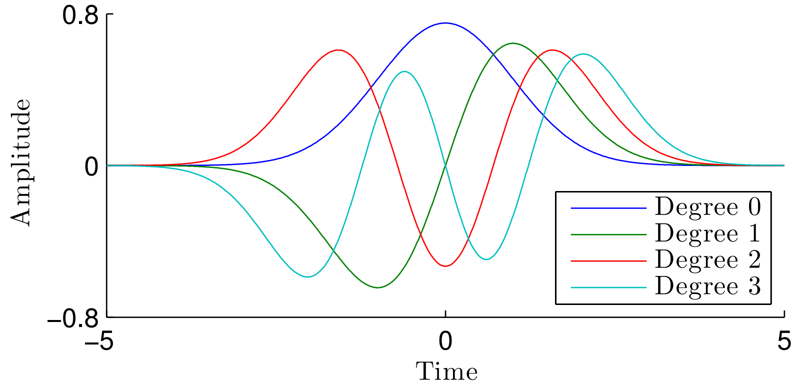

Figure 1.3: *The first four Hermite functions.*

decays exponentially, hence considerably faster than the $1/f$ decay of truncated sinusoids. This thesis will further investigate the use of Hermite functions in digital wireless communications.

Taking spectrum scarcity as a given, a few different situations regarding to wireless communications can be considered:

- Only a single user needs to transmit
- Multiple, mutually well-synchronized users share the spectrum
- Multiple users need to share the spectrum, but they are unsynchronized

The first situation excludes MAI because there are no other users to interfere with. Hence, spectral leakage is no problem. Considering that OFDM is capable of very high spectral efficiency, and thus large data throughput, when a large number of subcarriers is used, this scheme suits the situation properly. Moreover, it shows excellent robustness in frequency-selective channels, which are very often encountered in practice. The efficient implementation of OFDM using fast Fourier transform (FFT) algorithms also serves its applicability very well.

If there are multiple users and they are well-synchronized (second situation), OFDMA is a good choice, because interference between users is avoided by the synchronization. This way, all users combined can form one large OFDM system with different (sets of) subcarriers assigned to different users.

However, in case there are multiple users that are unsynchronized, while spectrum is scarce, an OFDM system is very undesirable. The spectral sidelobes of one user can easily interfere with others. The slow decay of spectral magnitude means that the frequency distance between different users needs to be large, which leads to inefficient use of the spectrum.

In this situation, communication based on Hermite functions is expected to be beneficial. The functions' rapid spectral decay allows efficient use of the spectrum, while a possibly modest spectral guard space provides robustness against missynchronization between users. Although the guard space lowers spectral efficiency, adapting it to the possible mismatches allows a minimum of efficiency loss, while MAI is still adequately mitigated.

1.4 Research goals and questions

The work done by Korevaar [23] was limited to theoretical analyses and simulations in a simple additive white Gaussian noise (AWGN) and Rayleigh-fading channel. Others, like Walton and Hanrahan [45], Haas and Belfiore [20] and Chongburee [9], have also performed only theoretical work on the subject of Hermite-based communication. However, the idea of actual data transmission through the air by a Hermite-based system is an exciting one. It would be very interesting to see whether transmission using this system actually works in practice. Moreover, many people confer great value to empirical results. This has led us to believe that experiments using actual radio transceivers can be worth while, despite the fact that there exist models for many (significant) real-world effects yielding very realistic simulation results. The first goal at the start of this thesis, therefore, is to conduct real-world experiments, in order to verify theoretical and simulated performance of Hermite-based communication.

Hermite functions decay exponentially, which means the decay is rapid but also that the non-zero tails are of infinite length. While OFDM symbols are strictly limited in time and have non-overlapping time slots, Hermite-based symbols will naturally overlap and suffer from ISI. Avoiding this overlap by truncation is not desirable, as it would introduce spectral sidelobes. The similar shapes in both the time domain and the frequency domain, cause the Hermite functions to have overlapping tails in both domains as well.

Because closer spaced symbols yield higher data throughput but also cause more mutual interference and thus data errors, the main research question arises: How dense can the symbols of a Hermite-based communication system be packed in time-frequency, when the BER is constrained? And immediately the question can be extended: How well is its spectral efficiency compared to e.g. OFDM? Furthermore, in the context of spectrum-scarce, multi-user communication, it will be interesting to know, how tolerant the system is to missynchronization between different transmitters and how this compares to OFDM/OFDMA.

1.5 Thesis outline

Chapter 2 presents and discusses (mostly existing) theoretical knowledge about the subject of this thesis. It presents mathematical models that are used in subsequent chapters and provides the definition of what is central to our research: the Hermite functions. After this, chapter 3 presents an analysis of multi-carrier communications where ISI is present, with a focus on Hermite-based systems. Details of the practical setup used for simulations and measurements are presented in chapter 4. Chapter 5 presents and discusses results from the simulations and measurements and links them to theory and analysis. Finally, in chapter 6, the most important conclusions of this thesis are given and directions for future research are recommended.

Chapter 2

Background theory

The current chapter provides a theoretical foundation for subsequent chapters to build upon. The lowpass signal representation, which is used widely in telecommunication theory, is introduced and a few of its advantages are noted. Also the notion of signal modulation for information carriage is explained, including mathematical equations that describe the process. A few important effects on signals in a wireless channel are described in the section on channel models. Furthermore, the time-frequency perspective, which is very convenient in reasoning about transmission signals and spectral usage, is treated briefly.

Essential in this thesis' subject are Hermite functions. Their mathematical definition is given in this chapter and a few notable properties are discussed. Furthermore, a derived set of signals, called the Fourier-Hermite signal set, is described. The chapter will conclude with a mathematical description of multiple transmitters and receivers.

Many functions (such as a transmitted signal $s_{\mathrm{tx}}(t)$) and variables are used in different situations throughout this thesis with a similar meaning but not identical definition. Strictly speaking, these functions and variables should receive a different name each time they are used for a different, specific case. However, to keep mathematical equations readable, we have avoided the subscripts and other elaborate notations that would be needed to differentiate between the specific situations. In stead, the specific instances of these functions and variables are distinguished by means of the surrounding text.

2.1 Fourier transform

The Fourier transform is an important tool within the context of this thesis. Several slightly different definitions of this mathematical operation are used in literature. Throughout this thesis, the *unitary* Fourier transform is used, unless explicitly indicated otherwise. The (forward) unitary Fourier transform ($\mathcal{F}$) and its inverse ($\mathcal{F}^{-1}$) are defined as

$$\mathcal{F}\Big\{f(t)\Big\} \triangleq \frac{1}{\sqrt{2\pi}} \int_{-\infty}^{+\infty} f(t)e^{-j\omega t}\,\mathrm{d}t \tag{2.1a}$$

$$\mathcal{F}^{-1}\Big\{F(\omega)\Big\} \triangleq \frac{1}{\sqrt{2\pi}} \int_{-\infty}^{+\infty} F(\omega)e^{j\omega t}\,\mathrm{d}\omega \tag{2.1b}$$

where $F(\omega) = \mathcal{F}\Big\{f(t)\Big\}$ is the frequency-domain[1] representation of $f(t)$. The often-used, non-unitary Fourier transform differs from Equation 2.1 by leaving out the factor $1/\sqrt{2\pi}$ in the forward transform and replacing it by $1/2\pi$ in the inverse transform.

The unitary Fourier transform is used here, because it is consistent with the fractional Fourier transform (FrFT), which will be introduced in section 2.7. Furthermore, Parseval's identity does not

[1]The Fourier transform is often considered a transform between the time and frequency domains, like in this thesis. However, other pairs of domains exist, that are related by the Fourier transform as well.

need a scaling factor:

$$\int_{-\infty}^{+\infty} \left|f(t)\right|^2 \,\mathrm{d}t = \int_{-\infty}^{+\infty} \left|F(\omega)\right|^2 \,\mathrm{d}\omega \tag{2.2}$$

The left-hand side of this equation corresponds to the common definition of signal energy. Hence, energy can be calculated from either the time-domain or frequency-domain representations of a signal without the inconvenience of additional scaling.

2.2 Bandpass and lowpass signal representations

Wireless communications systems operate on a certain carrier frequency in the radio-spectrum, meaning that the transmitted signals use a part of the spectrum close to that frequency. This part can be a band around the carrier frequency, as in basic amplitude modulation (AM) and frequency modulation (FM), or e.g. a band at one side of the carrier (single sideband (SSB)).

Most systems transmit signals that can be categorized as *narrowband bandpass* signals [39], occupying a band around a carrier frequency, with a bandwidth that is much smaller than the carrier frequency. It is usually (mathematically) convenient to reason about signals with their active band around direct current (DC), considering only the *equivalent lowpass* signals. Essentially, the two representations are frequency-translated versions of each other. The lowpass signal representation provides an abstraction from actual RF practicalities.

A complex-valued lowpass signal can be expressed in a Cartesian or a polar form:

$$s_{\mathrm{lp}}(t) = x(t) + jy(t) \tag{2.3a}$$

$$s_{\mathrm{lp}}(t) = a(t)\,\mathrm{e}^{j\Theta(t)} \tag{2.3b}$$

where $x(t)$, $y(t)$, $a(t)$ and $\Theta(t)$ are real-valued low-frequency functions. The signal $a(t)$ is the (magnitude) envelope and $\Theta(t)$ the phase of s_{lp}. The relations between the Cartesian and polar forms are the same as for regular complex values:

$$a(t) = \sqrt{x^2(t) + y^2(t)} \tag{2.4a}$$

$$\Theta(t) = \arg\left(\frac{y(t)}{x(t)}\right) \tag{2.4b}$$

The corresponding bandpass signal is the lowpass signal translated in frequency by F_{C}, the carrier frequency, and converted to a real-valued signal:

$$s_{\mathrm{bp}}(t) = \mathcal{R}\left\{s_{\mathrm{lp}}(t)\,\mathrm{e}^{j2\pi F_{\mathrm{C}}t}\right\} \tag{2.5}$$

This equation can be expanded to

$$s_{\mathrm{bp}}(t) = x(t)\cos\left(2\pi F_{\mathrm{C}}t\right) - y(t)\sin\left(2\pi F_{\mathrm{C}}t\right) \tag{2.6a}$$

or

$$s_{\mathrm{bp}}(t) = a(t)\cos\big(2\pi F_{\mathrm{C}}t + \Theta(t)\big) \tag{2.6b}$$

The cosine and sine carrier components are in phase quadrature and $x(t)$ and $y(t)$ are the *quadrature components* of the bandpass signal $s_{\mathrm{bp}}(t)$. Another name for $s_{\mathrm{lp}}(t)$ is the *complex envelope* of $s_{\mathrm{bp}}(t)$.

In addition to providing a convenient abstraction for theoretical reasoning, the lowpass signals are often physically present in communication systems. They are then commonly named *baseband* signals and the bandpass signals can be referred to as RF signals.

A transmitter can generate the lowpass signal in the digital domain, after which $x(t)$ and $y(t)$ are separately converted to the analog domain. In the analog domain, multiplication by cosine and sine carrier signals is performed and the results are summed, giving the real-valued bandpass signal.

The corresponding receiver multiplies the received bandpass signal with cosine and sine carrier signals of the same frequency and filters the results in the analog domain. This filtering is necessary to remove signal copies around $2F_{\mathrm{C}}$ resulting from the multiplication. The two filter outputs again represent (estimates of) $x(t)$ and $y(t)$ that are converted into the digital domain by analog-to-digital

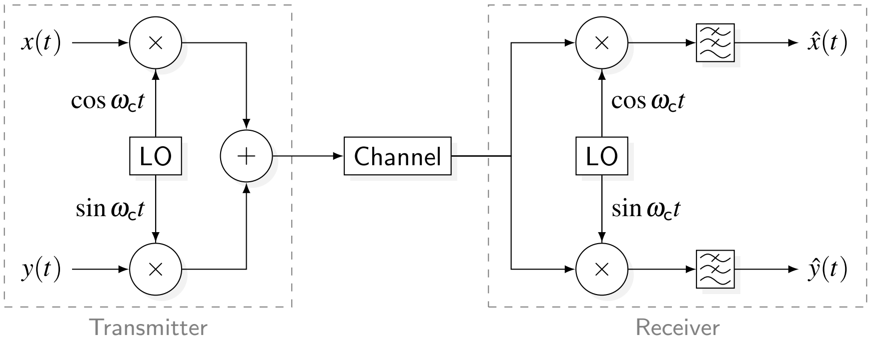

Figure 2.1: *Block diagram showing the conversions between baseband and RF signals in a radio system. The carrier frequency is ω_c.*

converters (ADCs). This simultaneous sampling of the *in-phase* (I) signal $x(t)$ and the *quadrature* (Q) signal $y(t)$ is often called *I/Q sampling*. The principle is shown as a block diagram in Figure 2.1.

The RF signal actually travels through the wireless channel, but channel effects manifest in the lowpass signals as well. Hence, an equivalent lowpass description of the channel can be made. An ideal channel at RF is also represented by an ideal channel at baseband, in which case the system provides a transparent connection between the transmitting and receiving baseband systems.

Simulation of communication systems including RF signals, requires the sample rate to accomodate these high-frequency signals without aliasing. It is more efficient to include only lowpass signal representations for simulation, because the sample rate can be considerably lower.

Unless explicitly indicated, the lowpass representation for signals and systems is used throughout this thesis.

2.3 Modulation schemes

Composing the lowpass signal at a (single-carrier) digital transmitter is in a simple form commonly represented by summing a series of time-shifted waveforms or *pulses* of a particular (complex) amplitude:

$$s_{\text{tx}}(t) = \sum_n A_n s_{\text{pulse}}(t - nT_{\text{sym}}) \tag{2.7}$$

where A_n is a (complex) amplitude or *modulation factor* corresponding to the employed modulation scheme, $s_{\text{pulse}}(t)$ is the basis pulse function (e.g. a rectangular pulse) and T_{sym} is the average *symbol duration*. A symbol is in this case composed of a single pulse, representing the information of one or more bits.

An estimate of the original modulation factor can be found at the receiver using a *matched filter* operation:

$$\hat{A}_n = \int_{-\infty}^{+\infty} s_{\text{rx}}(t)\overline{s_{\text{pulse}}(t - nT_{\text{sym}})}\, \mathrm{d}t \tag{2.8}$$

where the original (unmodulated) pulse function is used as a template function for the filter. The matched filter is the optimal demodulator for AWGN channels (see also subsection 2.5.2): it maximizes the signal-to-noise ratio (SNR) at the demodulator output.

Because Equation 2.7 describes a linear relationship, the spectrum of the basis pulse determines the spectrum of the transmitted signal. Often a rectangular basis pulse (of duration T_{sym}) is used, having the well-known sinc-shaped magnitude spectrum.

The employed modulation scheme defines the mapping of bit values to modulation factors. Binary phase shift keying (BPSK) maps a single bit of value 0 or 1 to a modulation factor of value -1 or 1, whereas quadrature phase shift keying (QPSK) maps in a similar fashion one bit to the real part of the modulation factor and another to the imaginary part. In generic form, M-phase shift keying (PSK) and M-quadrature amplitude modulation (QAM) map the values of $\log_2(M)$ bits to one modulation factor, where M is an integer number, usually a power of two. Each modulation factor can have one of M possible values. The values of modulation factors can be visualized by points in the complex plane, resulting in a *constellation diagram*.

The estimated modulation factors at the receiver are versions of the transmitted factors that are altered by the channel. Various channel effects result in different alterations of the modulation factors. If the channel exhibits additive noise, so do the received modulation factors. Attenuation reduces the magnitude of the modulation factors and a phase shift of the RF signal results in a static rotation of the constellation points around the origin.

The receiver makes a decision which original modulation factor value was transmitted. A simple method is to use strictly defined areas around each constellation point. The area within which the received modulation factor falls, determines the data. A data error occurs when a modulation factor was altered severely enough to fall in a different area. For schemes with multiple bits per modulation factor, Gray encoding is often used to assign the possible data values to modulation factors. This way, the most likely decision errors (the point falls in the area of an adjacent constellation point) result in only a single bit error [39].

The following equations describe QPSK mapping:

$$A_n = \sqrt{2}\left(b_{2n} - \frac{1}{2} + j\left(b_{2n+1} - \frac{1}{2}\right)\right) \tag{2.9a}$$

$$\hat{b}_{2n} = \begin{cases} 1 & \text{if } \mathcal{R}\{\hat{A}_n\} > 0 \\ 0 & \text{otherwise} \end{cases} \qquad \hat{b}_{2n+1} = \begin{cases} 1 & \text{if } \mathcal{I}\{\hat{A}_n\} > 0 \\ 0 & \text{otherwise} \end{cases} \tag{2.9b}$$

where b_n is the n^{th} bit, A_n is the n^{th} modulation factor, and $\hat{b}_n$ and $\hat{A}_n$ are the estimates of the n^{th} bit and modulation factor, respectively. The decision boundaries are the real and imaginary axes in the constellation diagram.

2.4 Multi-carrier systems

Many digital communication systems employ multiple carriers that are modulated and transmitted simultaneously. This means that one symbol is the sum of multiple, individually modulated, basis pulses with equal time shifts. The corresponding equations for transmitter and receiver are

$$s_{\text{tx}}(t) = \sum_{n} \sum_{k=0}^{N_{\text{c}}-1} A_{n,k} s_{\text{base},k}(t - nT_{\text{sym}}) \tag{2.10}$$

$$\hat{A}_{n,k} = \int_{-\infty}^{+\infty} s_{\text{rx}}(t) \overline{s_{\text{base},k}(t - nT_{\text{sym}})} \, \mathrm{d}t \tag{2.11}$$

where N_{c} is the number of subcarriers, $A_{n,k}$ is the modulation factor for subcarrier k in symbol n and $s_{\text{base},k}(t)$ is the basis signal for subcarrier k. The basis signals can be any set of functions that are sufficiently distinguishable at the receiver.

In AWGN channels (see also subsection 2.5.2), orthogonal function sets are optimum as basis functions [27]. Two functions $f(t)$ and $g(t)$ are orthogonal (over the interval $[-\infty, +\infty]$) when their inner product is zero:

$$\int_{-\infty}^{+\infty} f(t)\, \overline{g(t)} \, \mathrm{d}t = 0 \tag{2.12}$$

An orthogonal function set satisfies this criterion for every pair of distinct functions in the set.

OFDM employs a set of orthogonal complex exponentials as basis signals:

$$s_{\text{base},k}(t) = \begin{cases} \frac{1}{\sqrt{T_{\text{sym}}}} \mathrm{e}^{j2\pi kt/T_{\text{sym}}} & \text{if } 0 \leq t < T_{\text{sym}} \\ 0 & \text{otherwise} \end{cases} \tag{2.13}$$

where $k \in \mathbb{Z}$ denotes the subcarrier number. This results in a set of subcarriers at baseband frequencies k/T_{sym}. The total occupied bandwidth is subdivided into N_{c} bands.

Each basis signal of Equation 2.13 is essentially a complex exponential with frequency k/T_{sym}, multiplied with a rectangular window function of duration T_{sym}. The spectrum of a subcarrier is therefore sinc-shaped and centered at k/T_{sym}. Hence, the transmitted spectrum of an OFDM system is the sum of multiple, uniformly spaced, sinc pulses.

When compared to single-carrier transmission, the symbol time of OFDM is N_{c} times as long for the same throughput, reducing the impact of delay spread from e.g. multipath propagation (see subsection 2.5.3) [11]. In order to further mitigate ISI as well as ICI due to the delay spread, a cyclic prefix (CP) is often inserted before each symbol [32], at the cost of a longer total symbol time and thus lower throughput.

The subbands of OFDM are usually narrow enough to encounter an approximately flat frequency response in frequency-selective channels, reducing the required equalization at the receiver to a simple attenuation and phase rotation per subcarrier. Generating and modulating the subcarriers is often realized in hardware with the implementation of an (inverse) FFT algorithm.

2.5 Channel models

The bandpass signal from the transmitter passes through a — wired or wireless — channel, before arriving at the receiver. In an ideal channel, the signal remains untouched while propagating through the channel. But in practice, propagation effects and electromagnetic disturbances distort the signal in various ways.

2.5.1 Single-path loss

An important channel effect is path loss. This is noticable by a decrease in received signal power, when the distance between transmitter and receiver is increased.

One of the simplest mathematical models of the free-space loss is Friis' law [32][16]:

$$P_{\text{rx}} = \left(\frac{\lambda}{4\pi d}\right)^2 P_{\text{tx}} \tag{2.14}$$

in which P_{rx} and P_{tx} are the received and transmitted signal powers, respectively, λ is the wavelength of the signal and d is the distance between the antennas. The law assumes that there is only a line of sight (LOS) path for the electromagnetic wave to travel and that the antennas radiate isotropically. These assumptions are seldomly justified for practical situations, which is explained further in subsection 2.5.3. Furthermore, the law may only hold in the so-called far field of the antennas, meaning that all of the following conditions must be met [32]:

$$\begin{aligned} & d > d_R = \frac{2L_a^2}{\lambda} \\ & d \gg \lambda \\ & d \gg L_a \end{aligned}$$

in which d_R is called the Rayleigh distance and L_a is the largest physical dimension of the antenna.

In simulations of a communications system, using only the path-loss model for the channel normally makes little sense, if all other parts of the simulated system are ideal and simulation is performed with sufficient numerical precision.

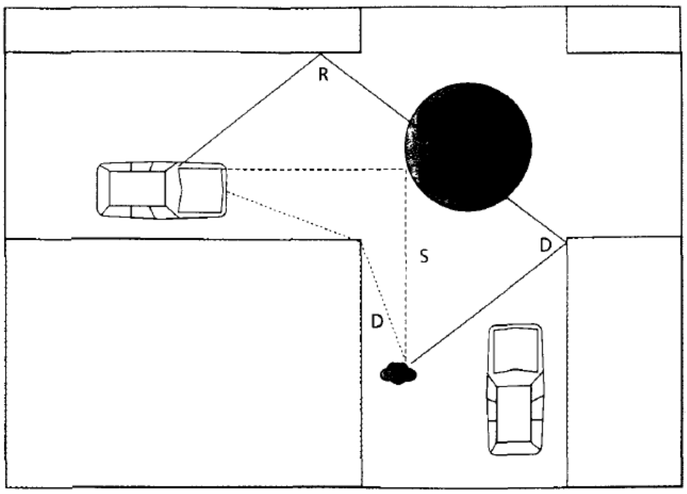

Figure 2.2: *Illustration of multipath propagation by reflection (R), scattering (S) and diffraction (D) (image from [5])*

2.5.2 AWGN

Another effect of a practical channel is the presence of noise. A noisy channel is often described by an AWGN channel model:

$$s_{\mathrm{rx}}(t) = \alpha s_{\mathrm{tx}}(t) + s_{\mathrm{n}}(t) \tag{2.15}$$

where $s_{\mathrm{tx}}(t)$ and $s_{\mathrm{rx}}(t)$ are the transmitted and received signals, respectively, α is the linear gain of the channel and $s_{\mathrm{n}}(t)$ is the added noise.

The value for α may be estimated with a path loss model such as Friis' law. It may optionally have a complex value, to model both attenuation and phase rotation.

The noise component is considered a complex-valued, zero-mean Gaussian noise process with a flat power spectral density (PSD) of N_0 (expressed as a power per unit bandwidth, e.g. W/Hz), so $\sigma^2 = N_0/2$ per dimension [29]. In practice, the total noise is dominated by the thermal noise introduced in the receiver circuitry [42]. Therefore, N_0 is dependent on the temperature by $N_0 = k_{\mathrm{B}}T_{\mathrm{e}}$ [32], where k_{B} is Boltzmann's constant and T_{e} is the environmental temperature. A commonly used value for approximate calculations is $N_0 = -174\mathrm{dBm/Hz}$.

2.5.3 Fading

Although fading channels are not actually used in the simulations of this thesis, wireless communications systems often employ techniques to combat their impairing effects. Furthermore, basic knowledge of the subject helps to hypothesize about the performance of a given system in practical situations. For these reasons, the current subsection focuses on fading channels.

In general, the propagation of radio waves is influenced by reflection, diffraction and scattering [5]. These main basic propagation mechanisms are illustrated in Figure 2.2. Each time an electromagnetic wave hits an object, one of these effects occurs. If the object has a smooth surface that is large in comparison to the wavelength, reflection occurs. However, objects with a rough surface or with dimensions in the order of the wavelength or smaller, cause scattering of the wave. A large object with a dense body causes secondary waves to appear on its other side, which is referred to as diffraction. A wave's path from transmitter to receiver, is likely to break more than once under the influence of these mechanisms, depending on the spatial positions of the transmitter, receiver and interacting objects (IOs).

For a given distance between transmitter and receiver, the attenuation can be different if objects are positioned differently, so attenuation of the signal is not only dependent on distance as in the free-space model. This is often modeled as a log-normally distributed variation about the mean

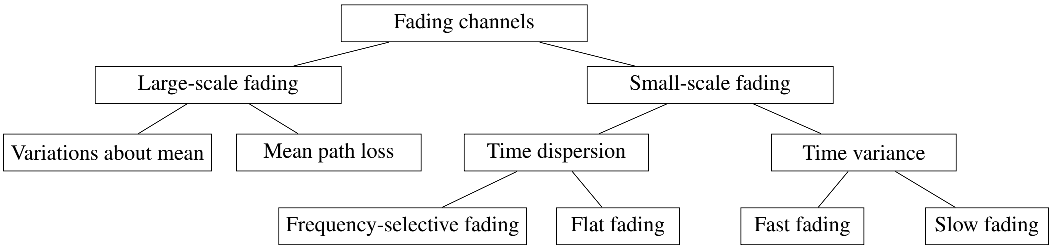

Figure 2.3: *Categorization of fading channel types (based on [42]).*

attenuation [42]. Combined with the mean path loss, this effect is called *Large-scale fading*, referring to the scale of object displacement, which is typically larger than the signal wavelength.

Another type of fading arises when there is more than one path from transmitter to receiver for a certain spatial arrangement, referred to as *multipath* propagation. The three mechanisms mentioned above cause the transmitted signal to be received multiple times, through different paths, when there are IOs. The paths have different attenuations and lengths, causing different received signal strengths and arrival times.

A result is *small-scale fading*: the received power can fluctuate heavily for different positions within a small area (about a half wavelength), significantly faster than for *large-scale fading*. Usually, in practice, there are enough IOs between transmitter and receiver to block a LOS path. If this is the case and the number of other paths is large, the received signal magnitude behaves like Rayleigh distributed noise during small-scale movement. Hence, the name *Rayleigh fading* is often used. But if a LOS path is present, its magnitude is often dominant in the received signal, changing the effects of multipath propagation. In the general case when a single dominant signal is present, the magnitude of the received signal has a Rician distribution and the name *Rician fading* is often used [42].

Small-scale fading causes time dispersion: the received signal looks like a 'smeared out' or time-scattered version of the source when viewed in the time domain. The summation of the differently delayed signals causes a filtering effect, i.e. the frequency response of the channel is not flat. However, signals with a very narrow bandwidth, i.e. smaller than the *channel coherence bandwidth*, encounter an approximately flat response. In this case, the small-scale fading channel is deemed *frequency-nonselective* or *flat fading*. For signal bandwidths larger than the coherence bandwidth, the frequency-dependent attenuation can be of significance and the channel is considered *frequency-selective fading*.

Movements of the transmitter, receiver or IOs cause variations in the channel properties, making the channel time-variant. The variations may be significant within the time interval of one symbol, which is called *fast fading*. In this case, the symbol time is larger than the *channel coherence time*. On the other hand, *slow fading* means that channel properties barely change during the transmission of one symbol, i.e. the symbol time is smaller than the coherence time.

In addition to the described magnitude variations, the movement causes Doppler shifts, which are most prominent in a fast fading channel. Doppler shifts can cause frequency missynchronization between transmitter and receiver devices.

The categorization of the fading channels is illustrated in Figure 2.3.

2.6 Probability of bit errors in AWGN

It is often acceptable to assume that in digital transmission, the source bits take either bit value with the same probability, i.e. $P(b_n = 1) = P(b_n = 0) = \frac{1}{2}$ for all $n \in \mathbb{Z}$. When transmitting data with BPSK modulation through an AWGN channel, the probability of a received bit error is given by [39]

$$P_\mathrm{b} = Q\left(\sqrt{\frac{2E_\mathrm{b}}{N_0}}\right) \tag{2.16}$$

where the Q-function $Q(x) = \frac{1}{\sqrt{2\pi}}\int_x^{+\infty} \mathrm{e}^{-t^2/2}\,\mathrm{d}t$ for $x \geq 0$, and E_b is the average bit energy. This holds only when no other sources for bit errors are present, such as interference. For a transmission of an infinite number of bits, the bit error probability is equal to the average BER [32].

The same equation is generally used for QPSK modulation. In that case, it is assumed that only the most likely errors occur, i.e. impairment of each modulation factor causes it to cross at most one decision boundary [39].

The (average) bit energy E_{b} is dependent on the modulation scheme and the energy of the basis signals. Assuming QPSK as described by Equation 2.9a and equal energy for all basis signals, the bit energy equals half the energy of the basis signals:

$$E_{\mathrm{b}} = \frac{1}{2} \int_{-\infty}^{+\infty} \left| s_{\mathrm{base},k}(t) \right|^2 \, \mathrm{d}t \tag{2.17}$$

for any valid value of k for the definition of the basis signal set.

2.7 Time-frequency analysis

In communications systems engineering it is very common to consider the spectral content of a signal. Spectral analysis gives information on properties such as the bandwidth that is occupied by the signal. The Fourier transform is the core operation used to transform a signal from the time domain to the frequency domain.

The time-domain signal representation gives information on the signal's behavior (instantaneous amplitude) over time. Similarly, the frequency-domain representation describes spectral content of the signal. Neither offers a view on how the spectral content changes over time, although this information is very desirable in many situations. For CR, the knowledge of the temporal changes in spectral content offers opportunities to detect present and past spectrum holes. But also for (digital) communication systems in general, a time-frequency perspective allows the designation of areas in time-frequency where a symbol is transmitted. Hence, optimization of data throughput, given certain bounds on time and frequency usage, would become a packing problem in two-dimensional space.

A paradox that arises in this context stems from the dependency of a periodic signal on the progression of time: an instantaneous frequency can not exist. Therefore, spectral analysis, and also time-frequency analysis, always involves observation of a signal over a certain time interval.

A well-known and widely used method for time-frequency analysis is the short-time Fourier transform (STFT), which is defined as

$$S_{\mathrm{st}}(t,\omega) \triangleq \frac{1}{\sqrt{2\pi}} \int_{-\infty}^{+\infty} s(\tau) g(\tau - t) \mathrm{e}^{-j\omega\tau} \, \mathrm{d}\tau \tag{2.18}$$

The result is the time-frequency representation $S_{\mathrm{st}}(t,\omega)$ of the time-domain signal $s(t)$.

Compared to the Fourier transform, Equation 2.18 adds the window function $g(t)$, that realizes the time-localized evaluation of spectral content. The best window function to use, depends on signal characteristics such as how rapid the spectral content changes, and on the demands for time and frequency resolutions, because of their inherent tradeoff [12].

A window function is not required for the Wigner-Ville distribution, which is defined as [12]

$$W(t,\omega) \triangleq \frac{1}{2\pi} \int_{-\infty}^{+\infty} s\left(t + \frac{\tau}{2}\right) \overline{s\left(t - \frac{\tau}{2}\right)} \mathrm{e}^{-j\omega\tau} \, \mathrm{d}\tau \tag{2.19}$$

The absense of a window function and other parameters conveniently avoids the need for tuning when analyzing arbitrary signals. A known problem with this distribution is that it sometimes shows spurious non-zero intensities in the time-frequency plane where zero intensity would be expected from prior knowledge of the analyzed signal [12]. This should be kept in mind when observing results from the distribution.

The FrFT is a generalization of the Fourier transform that can be interpreted as a rotation around the origin in the time-frequency plane, illustrated in Figure 2.4. The angle over which the rotation

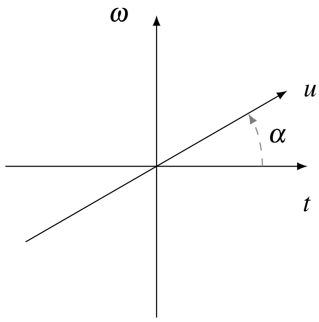

Figure 2.4: *Illustration of FrFT interpreted as rotation by angle α in the time-frequency plane.*

takes place is the parameter α. The FrFT is defined as [3]

$$\mathcal{F}^{\alpha}\Big\{f(t)\Big\} \triangleq \begin{cases} \sqrt{\frac{1-j\cot\alpha}{2\pi}}\, \mathrm{e}^{j\frac{\omega^2}{2}\cot\alpha} \int_{-\infty}^{+\infty} f(t)\, \mathrm{e}^{j\frac{t^2}{2}\cot\alpha}\, \mathrm{e}^{jut\csc\alpha}\, \mathrm{d}t & \text{if } \alpha \text{ is not a multiple of } \pi \\ f(t) & \text{if } \alpha \text{ is a multiple of } 2\pi \\ f(-t) & \text{if } \alpha+\pi \text{ is a multiple of } 2\pi \end{cases} \tag{2.20}$$

where $F_\alpha(u) = \mathcal{F}^{\alpha}\Big\{f(t)\Big\}$. If the angle $\alpha = \pi/2$, the FrFT reduces to the normal (unitary) Fourier transform. This suits intuition perfectly, because the Fourier transform provides a signal representation along the frequency axis, which is perpendicular to the time axis in the time-frequency plane. Similarly, if $\alpha = -\pi/2$, one finds the inverse Fourier transform.

A review of various methods for time-frequency analysis besides the ones mentioned here can be found in [12], including quite elaborate mathematical comparisons. In this thesis, the theory of time-frequency representations is not elaborated further, because the perspective will be used mainly for illustrational purposes.

2.8 Hermite functions

Hermite functions are used in our research as a set of basis signals for multi-carrier communication. These functions are windowed and normalized Hermite polynomials. This section provides their mathematical definition and discusses a few notable properties.

2.8.1 Definition

Two similar definitions of Hermite polynomials can be found in literature. They are called in e.g. [10] and [23] the physicists' and probabilists' definitions. Mainly because of some convenient mathematical properties, the physicists' definition is used throughout this thesis, which is given in [23] as:

$$H_n(x) \triangleq (-1)^n e^{x^2} \frac{d^n}{dx^n}\left(e^{-x^2}\right) \tag{2.21}$$

where $n \in \mathbb{N}_0$ and denotes the degree of the polynomial. Upon substitution of n by a number and subsequent evaluation of the formula, the exponentials in the definition cancel and a polynomial remains.

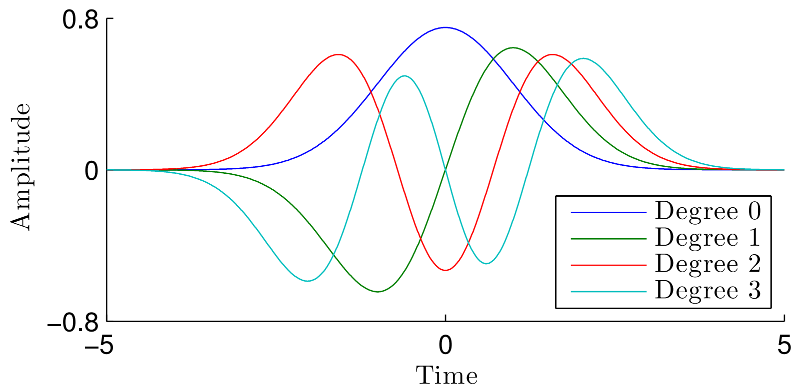

Figure 2.5: *Hermite functions of the first four degrees. The Hermite function of degree 0 is a Gaussian function.*

The Hermite polynomials of the first eight degrees are

$$\begin{aligned} H_0(x) &= 1 \\ H_1(x) &= 2x \\ H_2(x) &= 4x^2 - 2 \\ H_3(x) &= 8x^3 - 12x \\ H_4(x) &= 16x^4 - 48x^2 + 12 \\ H_5(x) &= 32x^5 - 160x^3 + 120x \\ H_6(x) &= 64x^6 - 480x^4 + 720x^2 - 120 \\ H_7(x) &= 128x^7 - 1344x^5 + 3360x^3 - 1680x \end{aligned} \tag{2.22}$$

A recurrence relation, suitable for numerical calculation of the polynomials, is [31]

$$H_{n+1}(x) = 2xH_n(x) - 2nH_{n-1}(x) \tag{2.23}$$

with initial conditions $H_0(x) = 1$ and $H_1(x) = 2x$.

To form the Hermite functions corresponding to the polynomials, the window function $g(x) = e^{-x^2/2}$ is used, along with the normalization factor $\sqrt{2^n n! \sqrt{\pi}}$. The window function causes the functions to have finite energy in an infinite interval and normalization ensures that this energy is unity for all functions of the family. The n^{th} order Hermite function is defined by

$$h_n(x) \triangleq \frac{1}{\sqrt{2^n n! \sqrt{\pi}}} e^{-x^2/2} H_n(x) \tag{2.24}$$

where $n \in \mathbb{N}_0$. Figure 2.5 shows a plot of the Hermite functions of the first four orders.

In this thesis, the Hermite functions are occasionally simply referred to as “Hermites”.

2.8.2 Properties

Both the Hermite polynomial and the Hermite function of degree n have n zero crossings. Furthermore, even orders result in even functions and odd orders in odd functions. These properties are clearly visible in Figure 2.5. Furthermore, the largest magnitude of a Hermite function occurs at the outer local (absolute) maxima, just before exponential decay sets in.

According to their second-order moments, the Hermite functions are time-frequency well-localized, with the function of degree 0, which is Gaussian, optimally localized. However, the spread of energy in time and frequency increases with function degree. This can be observed in Figure 2.5 by looking at the decay of the curves. The figure furthermore shows that for increasing degree, the peak values, which coincide with the outer local absolute maxima, decrease.

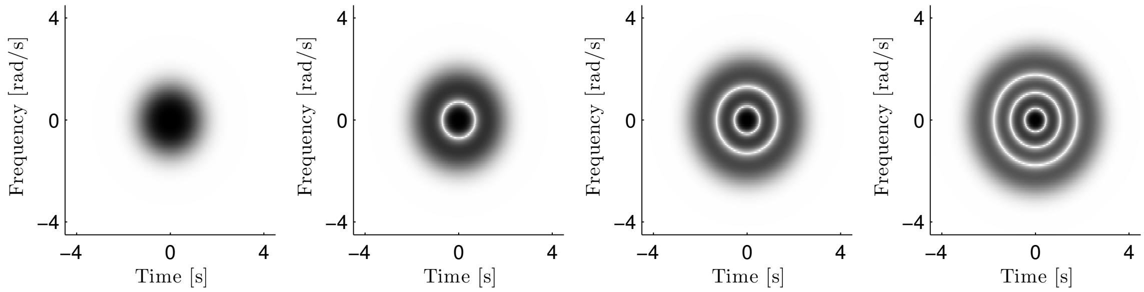

(a) *Degree 0* **(b)** *Degree 1* **(c)** *Degree 2* **(d)** *Degree 3*

Figure 2.6: *Time-frequency illustrations of the first four Hermite functions. The plots were obtained from the Wigner-Ville distribution (using [6]).*

The product of the second-order moments is a constant that depends on the function degree [23]:

$$\sqrt{\sigma_t^2 \sigma_\omega^2} = n + \frac{1}{2} \tag{2.25}$$

where σ_t^2 and σ_ω^2 are the variances in time and in frequency, respectively. This product is sometimes referred to as the time-bandwidth product (TBWP) [23] and is used as an indication of energy localization in time-frequency. The TBWP of equal-degree Hermite functions is constant, independent of time scaling, relating to a direct exchange between time and bandwidth.

As a set of functions, the Hermites are orthogonal over the interval $[-\infty, +\infty]$. Because of this, they are particularly suitable for multi-carrier communications in AWGN channels. However, two operations, that are needed for implementation in a communication system, reduce orthogonality:

1. A real communication system transmits for a limited amount of time and basis waveforms are limited in time as well. Truncation of Hermite functions is a cause for orthogonality loss.

2. To build multiple symbols for transmission, the basis waveforms are shifted in time and/or frequency according to each symbol's position in time-frequency. The Hermite functions in two sets, of which one set is shifted in time-frequency, are not orthogonal.

Loss of orthogonality between basis waveforms causes ICI, as different subcarriers become less distinguishable. The larger the truncation interval, the less orthogonality is lost. Therefore, it is important that this interval is taken sufficiently large, taking into account the larger spread of higher function degrees.

The loss of orthogonality between time-frequency-shifted Hermites leads to ISI, limiting transmission performance. For larger shifts in time-frequency, the loss of orthogonality is smaller, but symbol density is smaller as well. The smaller symbol density means a decrease of spectral efficiency. This trade-off is one of the main topics of the research described in this thesis.

Another important property of the Hermite functions is that they are eigenfunctions of the FrFT [23]:

$$\mathcal{F}^\alpha\Big\{h_n(t)\Big\} = \lambda_{n,\alpha}\, h_n(\omega) \qquad \text{with } \lambda_{n,\alpha} = \mathrm{e}^{-jn\alpha} \tag{2.26}$$

where $\lambda_{n,\alpha}$ is the corresponding (complex) eigenvalue, which reduces to $\lambda_{n,\pi/2} = (-j)^n$ for the non-fractional Fourier transform. Hence, Hermites are isomorphic under the (fractional) Fourier transform [30], i.e. the signal shape is the same in both the time and frequency domains and at every angle in the time-frequency plane.

The fact that the Hermite functions posses this property is important in our way of reasoning about the functions in time-frequency. Hermites exhibit a circular pattern in the time-frequency plane, as shown in Figure 2.6. The Hermites' magnitudes develop identical in all directions from the time-frequency origin, exhibiting the exponential tail as well. For reasoning about a Hermite signal, it can thus be represented by a circle that is actually a magnitude isoline. In the case of Hermite-based

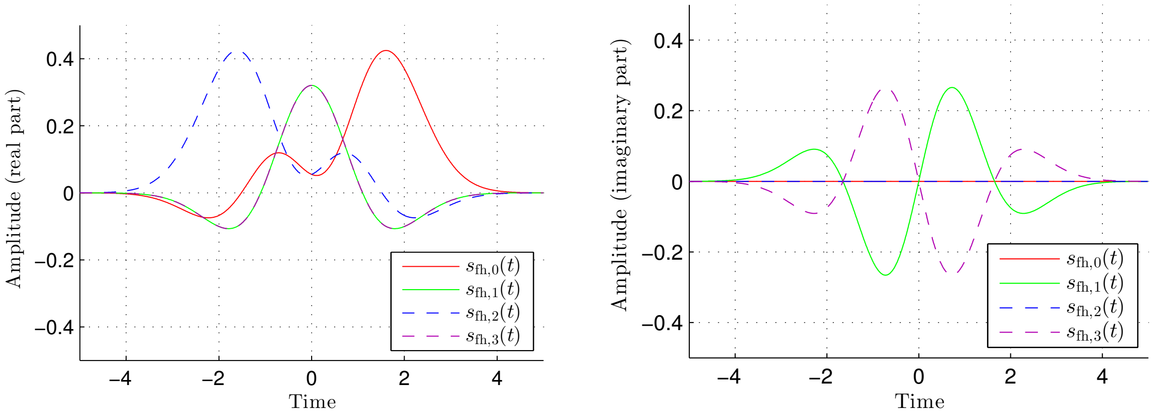

Figure 2.7: *Signals of the Fourier-Hermite set with $K = 4$. Real (left) and imaginary (right) parts shown separately.*

communications, the circle can be used to represent a symbol and a complete transmit signal can be represented by a collection of circles that are all uniquely time-frequency shifted.

With help of the time-scaling property of the Fourier transform and the fact that Hermites are eigenfunctions of the transform, the exchange between time and bandwidth is easily shown in an equation:

$$\mathcal{F}\left\{h_n\left(\frac{t}{\sigma_\mathrm{h}}\right)\right\} = \lambda_{n,\pi/2}\,\sigma_\mathrm{h}\,h_n\left(\sigma_\mathrm{h}\omega\right) \tag{2.27}$$

where σ_h is an arbitrary time-scaling factor.

2.9 Fourier-Hermite signals

Previous research has indicated that higher-order Hermite functions are very sensitive to time and/or frequency offsets [25] when employed as carriers for data transmission. In this thesis, it is assumed that transmitter and receiver are perfectly synchronized in time and frequency, avoiding problems caused by the offset sensitivity. Furthermore, the maximum number of subcarriers is sixteen, which is relatively low. By contrast, OFDM-based WLAN employs 52 (active) subcarriers [21].

As a potential solution for the time-frequency offset sensitivity, another set of basis signals for multi-carrier communications is proposed in [25]. Again based on Hermites, the signals are called Fourier-Hermite signals. Each signal in this set is a sum of multiple weighted Hermite functions. The weights correspond to sampled Fourier signals (complex exponentials), hence the name for the new signal set.

2.9.1 Definition

The set of Fourier-Hermite signals is defined as [25]

$$s_{\mathrm{fh},n}(t) \triangleq \frac{1}{K}\sum_{k=0}^{K-1} \mathrm{e}^{j2\pi\frac{kn}{K}}\,h_k\left(t\right) \tag{2.28}$$

with K the number of signals in the set and the signal index $n \in \{0, 1, ..., K-1\}$.

The time-domain representation of the signal set with $K = 4$ is shown in Figure 2.7.

2.9.2 Properties

The time-frequency representation of a Fourier-Hermite set shows a flower-like pattern, with the ‘leaves’ corresponding to the individual signals, as illustrated in Figure 2.8. Hence, it is clear that

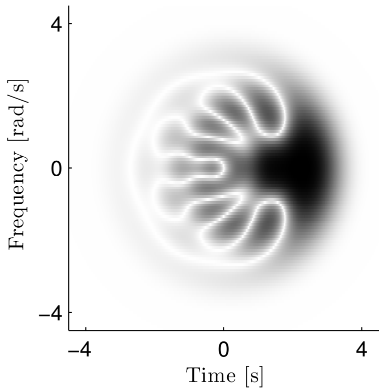

(a) *Signal 0*

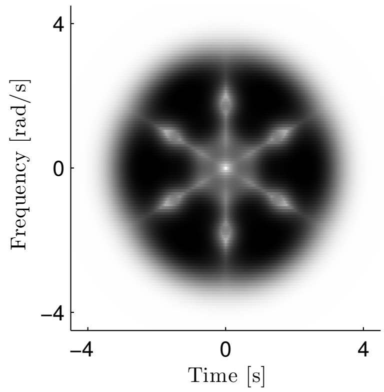

(b) *Full signal set (signal powers summed)*

Figure 2.8: *Time-frequency illustrations of the Fourier-Hermite signals for $K = 6$. The plots were obtained from the Wigner-Ville distribution (using [6]).*

the center of energy in time-frequency is different for each signal in the set. This is in contrast to Hermite functions, that all have the center at the origin of the time-frequency plane.

Regardless of the energy center, the time-frequency spread of a Fourier-Hermite signal around its center is not dependent on the signal index, but on the total number of signals in the set (K). This is again in contrast to the set of Hermite functions, that contains an infinite number of functions in the set. However, a complete Fourier-Hermite set is again well-localized in time-frequency [25].

Fourier-Hermite signals from the same set are mutually orthogonal over the interval $[-\infty, +\infty]$. Hence, a discussion similar to that given in subsection 2.8.2 with regards to orthogonality, applies to the Fourier-Hermite signals.

2.10 Symbol distributions

The equations for single-carrier systems in section 2.3 and multi-carrier systems in section 2.4 describe only a single transmitter-receiver pair. A more general description of (a collection of) digital transmitters and receivers using a single channel, can be obtained by considering separate symbols that are individually shifted in time-frequency. The transmitters can be described by

$$s_{\mathrm{tx}}(t) = \sum_{n} \sum_{k=0}^{N_{\mathrm{c}}-1} A_{n,k}\, s_{\mathrm{base},k}(t - \tau_n)\, \mathrm{e}^{j\nu_n t} \tag{2.29}$$

where τ_n and ν_n are the time- and frequency-shifts, respectively, of symbol n. Furthermore, the equation for the receivers (collectively) is

$$\hat{A}_{n,k} = \int_{-\infty}^{+\infty} s_{\mathrm{rx}}(t + \tau_n)\, \mathrm{e}^{-j\nu_n (t+\tau_n)}\, \overline{s_{\mathrm{base},k}(t)}\, \mathrm{d}t \tag{2.30}$$

where again the matched-filter is employed.

The above equations reduce to the multi-carrier-system equations Equation 2.10 and Equation 2.11 if $\tau_n = nT_{\mathrm{sym}}$ and $\nu_n = 0$. As an additional example, a second system, using a main carrier frequency Ω_2 above the first one, can be added by specifying $\tau_n = \left\lfloor \frac{n}{2} \right\rfloor T_{\mathrm{sym}}$ and $\nu_{2n'} = 0$, $\nu_{2n'+1} = \Omega_2$ with $n' \in \mathbb{Z}$. In this case, all even-indexed symbols belong to the first transmitter and all odd-indexed symbols to the second. However, in general, any symbol can come from an arbitrary transmitter.

In the context of the current research, it is convenient to deal with regular distributions of the symbols in time-frequency. A few relevant symbol distributions are shown in Figure 2.9. The first three distribute symbols uniformly along a single, straight line in time-frequency and are therefore considered one-dimensional distributions. In the current work, they are referred to as time-directed, frequency-directed and diagonally-directed distributions, because the line runs parallel to the time

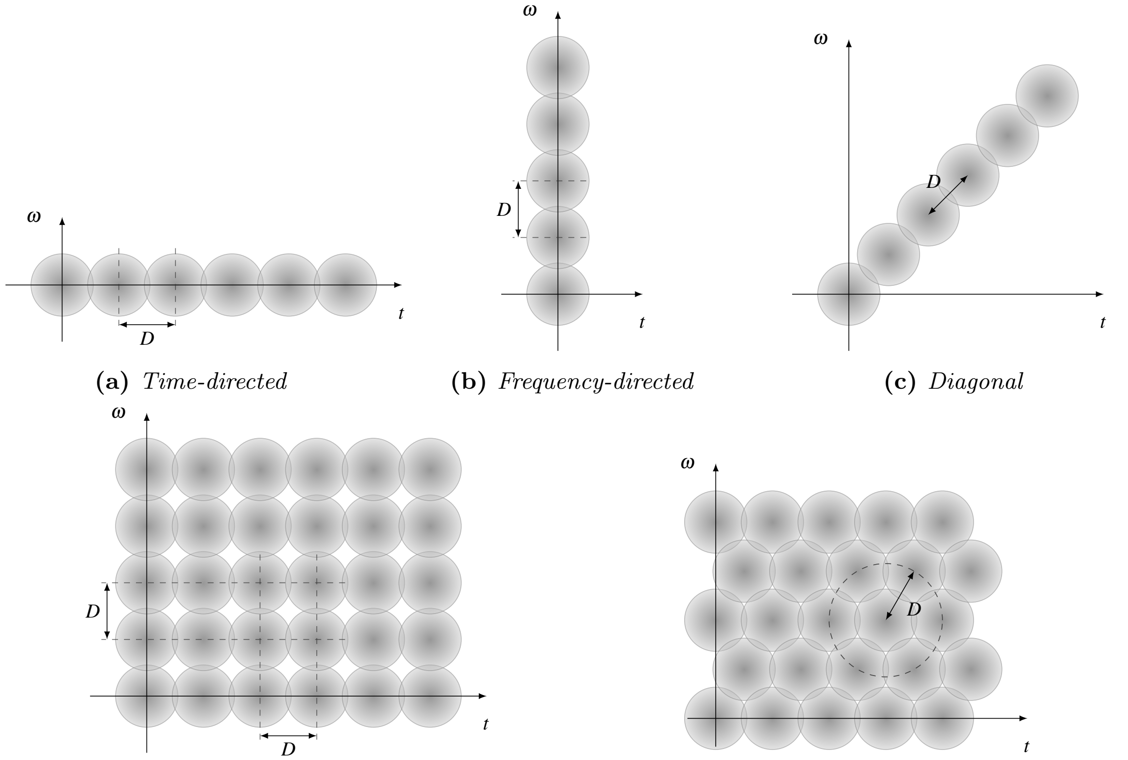

(a) *Time-directed* **(b)** *Frequency-directed* **(c)** *Diagonal*

(d) *Rectangular. Density is* $\frac{2\pi}{D^2}$ *symbols per sHz.* **(e)** *Hexagonal. Density is* $\frac{4\pi}{\sqrt{3}D^2}$ *symbols per sHz.*

Figure 2.9: *Illustrations of time-frequency symbol distributions.*

axis or the frequency axis or at an angle from the axes, respectively. A significant realistic meaning is not ascribed to the frequency-directed and diagonal distributions, as these are used as virtual test cases only. The last two distributions position the symbols not on a single line, but spread out in the time-frequency plane. Hence, they are considered two-dimensional distributions.

Assuming the distributions reach infinitely over the time-frequency plane, each symbol is adjacent to two, four or six other symbols for one-dimensional, rectangular and hexagonal distributions, respectively. The distance between the centers of symbols is equal for all adjacent symbols and is indicated in Figure 2.9, denoted by D.

Because a hexagonal grid yields optimal circle packing in a two-dimensional space [17], the hexagonal distribution gives optimal time-frequency symbol density, if the symbols are circular. It was seen in section 2.8 that Hermite functions exhibit a circular pattern in time-frequency. Therefore, the hexagonal symbol distribution is potentially useful for optimization of a Hermite-based transmitter's spectral efficiency.

The symbol densities (symbols per second-Hertz) for the two-dimensional symbol distributions are

$$\rho_{\text{rect}} = \frac{2\pi}{D^2} \tag{2.31}$$

$$\rho_{\text{hex}} = \frac{4\pi}{\sqrt{3}D^2} \tag{2.32}$$

In this chapter, an important part of the theoretical knowledge that is needed for the rest of this thesis, was presented. The next chapter will move on to analysing the subject and attempt to build a model that can help in the prediction of the performance of a Hermite-based communication system.

Chapter 3

Analysis

This chapter presents a theoretical analysis of the basic communications system defined in chapter 2. The goal is to gain insight in the behavior of OFDM and Hermite-based systems regarding ISI. This insight and the accompanying mathematical equations will be linked to the results of simulations and measurements in chapter 5. Furthermore, signal bandwidth and time-frequency usage of Hermite-based transmissions is discussed in preparation for the presentation of these results. The last point addressed in this chapter is the specification of a criterion on BER to serve as a reference point for transmission quality.

3.1 Interference caused by overlapping symbols

It was already noted that Hermite-based symbols in a communication system suffer from inherent ISI because relative shifting of the functions in time-frequency reduces orthogonality. The relative positions in time-frequency of any two symbols affect the exact effect of their mutual interference. In the current section this effect is investigated theoretically. First, we will derive an expression for the modulation factors at the receiver's demodulator output in terms of transmitted modulation factors.

Assuming an ideal noiseless channel, i.e. $s_{\mathrm{rx}}(t) = s_{\mathrm{tx}}(t)$, Equation 2.29 and Equation 2.30 can be combined, resulting in

$$\hat{A}_{n,k} = \int_{-\infty}^{+\infty} \left(\sum_{m} \left[\sum_{l=0}^{N_{\mathrm{c}}-1} A_{m,l}\, s_{\mathrm{base},l}(t + \tau_n - \tau_m) \right] \mathrm{e}^{j\nu_m (t+\tau_n)} \right) \mathrm{e}^{-j\nu_n (t+\tau_n)}\, \overline{s_{\mathrm{base},k}(t)}\, \mathrm{d}t \tag{3.1}$$

This can be rewritten to

$$\hat{A}_{n,k} = \sum_{m} \sum_{l=0}^{N_{\mathrm{c}}-1} A_{m,l}\, \mathrm{e}^{j\nu_{mn}\tau_n} \int_{-\infty}^{+\infty} s_{\mathrm{base},l}(t - \tau_{mn})\, \mathrm{e}^{j\nu_{mn} t}\, \overline{s_{\mathrm{base},k}(t)}\, \mathrm{d}t \tag{3.2}$$

where $\nu_{mn} = \nu_m - \nu_n$ and $\tau_{mn} = \tau_m - \tau_n$ for shorter notation. Clearly, the received modulation factor $\hat{A}_{n,k}$ is a sum of the transmitted modulation factors $A_{m,l}$, each multiplied by a particular (complex) value. This value depends on the time-frequency position of the symbol ($[\tau_n\ \nu_n]$) and the subcarrier number (k) that correspond to the observed modulation factor ($\hat{A}_{n,k}$) and the position and subcarrier number of the interferer. Define this complex multiplier as

$$\chi_{k,l,m,n} \triangleq \mathrm{e}^{j\nu_{mn}\tau_n} \int_{-\infty}^{+\infty} s_{\mathrm{base},l}(t - \tau_{mn})\, \mathrm{e}^{j\nu_{mn} t}\, \overline{s_{\mathrm{base},k}(t)}\, \mathrm{d}t \tag{3.3}$$

Using this definition, Equation 3.2 can be written in a convenient compact form:

$$\hat{A}_{n,k} = \sum_{m} \sum_{l=0}^{N_{\mathrm{c}}-1} A_{m,l}\, \chi_{k,l,m,n} \tag{3.4}$$

Hence, the received modulation factor can be seen as the weighted sum of all transmitted modulation factors of all symbols. The weights are the multipliers defined by Equation 3.3.

3.1.1 SIR

The signal-to-interference ratio (SIR) is a measure for the amount of interference a signal undergoes due to other signals. It is defined as the recovered transmitted-signal energy E_{sr}, divided by the total interference energy E_{i}, or, equivalently, the average recovered power of the desired signal P_{sr} divided by the average total interference power P_{i}:

$$\mathrm{SIR} \triangleq \frac{E_{\mathrm{sr}}}{E_{\mathrm{i}}} = \frac{P_{\mathrm{sr}}}{P_{\mathrm{i}}} \tag{3.5}$$

Assuming uncorrelated, uniformly distributed modulation factors at the transmitter, the (generalized) power of the received modulation factor is

$$\left|\hat{A}_{n,k}\right|^2 = \sum_{m} \sum_{l=0}^{N_{\mathrm{c}}-1} \left|A_{m,l}\, \chi_{k,l,m,n}\right|^2 \tag{3.6}$$

which is the sum of one desired term $\left|A_{n,k}\, \chi_{k,k,n,n}\right|^2$ and multiple interference terms. The ratio between the desired term and the interference terms is the SIR for this modulation factor:

$$\mathrm{SIR}_{n,k} = \frac{\left|A_{n,k}\, \chi_{k,k,n,n}\right|^2}{\left|\hat{A}_{n,k}\right|^2 - \left|A_{n,k}\, \chi_{k,k,n,n}\right|^2} \tag{3.7}$$

Assume N_{sym} symbols are transmitted, then the average SIR is

$$\mathrm{SIR}_{\mathrm{avg}} = \frac{1}{N_{\mathrm{sym}} N_{\mathrm{c}}} \sum_{n=0}^{N_{\mathrm{sym}}-1} \sum_{k=0}^{N_{\mathrm{c}}-1} \mathrm{SIR}_{n,k} \tag{3.8}$$

If N_{sym} is large and transmission modulation factors all have the same distribution with zero mean, then

$$\sum_{n=0}^{N_{\mathrm{sym}}-1} \sum_{k=0}^{N_{\mathrm{c}}-1} \left|A_{n,k}\, \chi_{k,k,n,n}\right|^2 \approx \sigma^2_{\mathrm{mod}} \sum_{n=0}^{N_{\mathrm{sym}}-1} \sum_{k=0}^{N_{\mathrm{c}}-1} \left|\chi_{k,k,n,n}\right|^2 \tag{3.9a}$$

$$\sum_{m=0}^{N_{\mathrm{sym}}-1} \sum_{l=0}^{N_{\mathrm{c}}-1} \left|A_{m,l}\, \chi_{k,l,m,n}\right|^2 \approx \sigma^2_{\mathrm{mod}} \sum_{m=0}^{N_{\mathrm{sym}}-1} \sum_{l=0}^{N_{\mathrm{c}}-1} \left|\chi_{k,l,m,n}\right|^2 \tag{3.9b}$$

where σ^2_{mod} is the variance of the transmitted modulation factors' probability distribution. The variance is now present as a factor in both the numerator and denominator of the SIR expression and therefore drops out of the equation. This results in

$$\mathrm{SIR}_{\mathrm{avg}} = \frac{1}{N_{\mathrm{sym}} N_{\mathrm{c}}} \sum_{n=0}^{N_{\mathrm{sym}}-1} \sum_{k=0}^{N_{\mathrm{c}}-1} \frac{\left|\chi_{k,k,n,n}\right|^2}{\left[\sum_{m=0}^{N_{\mathrm{sym}}-1} \sum_{l=0}^{N_{\mathrm{c}}-1} \left|\chi_{k,l,m,n}\right|^2\right] - \left|\chi_{k,k,n,n}\right|^2} \tag{3.10}$$

3.1.2 ISI in the time-directed symbol distribution

Consider the case of a single-dimension, time-directed symbol distribution. The value of T_{dist} is the center-to-center time distance between successive symbols. In this case, $\tau_n = nT_{\mathrm{dist}}$ and $\nu_n = 0$ are substituted into Equation 3.3, resulting in

$$\chi_{k,l,m,n} = \int_{-\infty}^{+\infty} s_{\mathrm{base},l}\big(t - (m-n)T_{\mathrm{dist}}\big)\, \overline{s_{\mathrm{base},k}(t)}\, \mathrm{d}t \tag{3.11}$$

which can be recognized as the cross-correlation function (CCF) of the basis functions $s_{\text{base},l}(t)$ and $s_{\text{base},k}(t)$. In general, the CCF of two complex-valued functions $f(t)$ and $g(t)$ is defined as

$$\gamma_{f,g}(t) \triangleq \int_{-\infty}^{+\infty} f(\tau)\overline{g(\tau - t)}\, \mathrm{d}\tau \tag{3.12}$$

So, by moving the term $(m-n)T_{\text{dist}}$ into the conjugate basis function's argument, we get

$$\chi_{k,l,m,n} = \gamma_{s_{\text{base},l},s_{\text{base},k}}\big((n-m)T_{\text{dist}}\big) \tag{3.13}$$

We see that in this case, the weights in Equation 3.4 are determined by the CCF of two basis signals: one corresponding to the received modulation factor and one corresponding to the interfering subcarrier. Each weight is the value of this CCF evaluated at the difference between the symbols' positions in time.

3.1.3 ISI in the frequency-directed symbol distribution

For the frequency-directed symbol distribution, a similar derivation can be made by substituting $\tau_n = 0$ and $\nu_n = n\Omega_{\text{dist}}$ into Equation 3.3. Now, Ω_{dist} is the center-to-center frequency distance between adjacent symbols. In this case, the modulation factor weight becomes

$$\chi_{k,l,m,n} = \int_{-\infty}^{+\infty} s_{\text{base},l}(t)\, \overline{s_{\text{base},k}(t)}\, \mathrm{e}^{-j(n-m)\Omega_{\text{dist}}t}\, \mathrm{d}t \tag{3.14}$$

exposing an operation similar to a Fourier transform, performed on the product of basis signal l and the conjugate of basis signal k, with $\omega = (n-m)\Omega_{\text{dist}}$. The Fourier transform property $\overline{f(t)} \leftrightarrow \overline{F(-\omega)}$ and the Fourier frequency-domain convolution theorem [7] (scaled for the unitary transform) allow rewriting this to

$$\chi_{k,l,m,n} = \gamma_{S_{\text{base},l},S_{\text{base},k}}\big((n-m)\Omega_{\text{dist}}\big)\, \mathrm{d}t \tag{3.15}$$

which has a shape similar to Equation 3.13. Now each weight of Equation 3.4 is determined by the CCF of the Fourier-transformed basis signals, evaluated at the difference between the symbols' positions in frequency.

3.1.4 ISI at an arbitrary direction in time-frequency

The time-directed and frequency-directed symbol distributions contain ISI in only one direction in the time-frequency plane. They are particular cases of ISI occurring in an arbitrary direction. For two-dimensional symbol distributions, the direction from which a particular symbol receives interference is different per interfering symbol. Given the forms of Equation 3.13 and Equation 3.15 it is not unlikely that for other directions, the equation will contain the CCF of the fractional-Fourier-transformed basis signals. The author has attempted to derive a convenient form of this generalized equation, but it has proven to be more involved than was anticipated. Therefore, it is not elaborated here.

However, given the fact that Hermite functions are eigenfunctions of the FrFT, it is expected that there is no difference in interference direction. We will see in the next section that the magnitude of the fractional-Fourier-transformed Hermites' CCF is also independent of the angle.

3.2 Basis signal cross-correlation functions

In the above derivations it has become clear that CCFs of the basis signals and of their (fractional) Fourier transforms are very useful for the analysis of ISI for overlapping symbols. Therefore those functions corresponding to the basis signals of choice deserve some more attention.

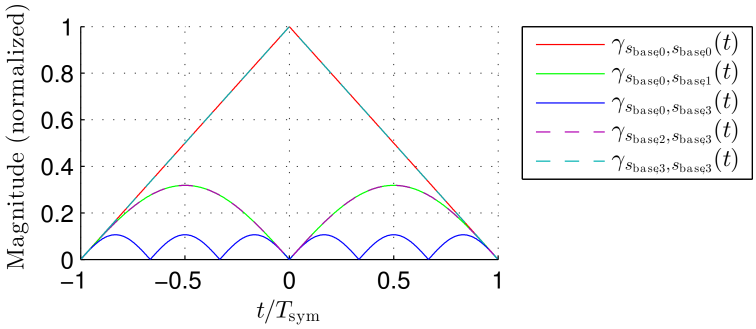

Figure 3.1: *Magnitude of a few OFDM basis signals' CCFs. The functions are zero for $|t/T_{sym}| > 1$. Peak magnitude is smaller for larger difference between k and l.*

3.2.1 CCFs of OFDM basis signals

OFDM uses (truncated) complex exponential basis signals as defined earlier (Equation 2.13), which are repeated here for convenience:

$$s_{\text{base},k}(t) = \begin{cases} \frac{1}{\sqrt{T_{\text{sym}}}} \mathrm{e}^{j2\pi kt/T_{\text{sym}}} & \text{if } |t| \leq \frac{T_{\text{sym}}}{2} \\ 0 & \text{otherwise} \end{cases} \tag{3.16}$$

The frequency-domain representations of these signals are

$$S_{\text{base},k}(\omega) = \mathcal{F}\Big\{s_{\text{base},k}(t)\Big\}(\omega) = \sqrt{\frac{T_{\text{sym}}}{2\pi}}\,\mathrm{sinc}\bigg(\frac{\omega T_{\text{sym}}}{2} - k\pi\bigg) \tag{3.17}$$

where $\mathrm{sinc}(x) = \frac{\sin x}{x}$ for $x \neq 0$ and $\mathrm{sinc}(0) = 1$.

The CCF of the time-domain representation is derived to be

$$\gamma_{s_{\text{base},k},s_{\text{base},l}}(t) = \begin{cases} \left(1 - \frac{|t|}{T_{\text{sym}}}\right) \mathrm{e}^{j2\pi kt/T_{\text{sym}}} & \text{if } k = l \text{ and } |t| \leq T_{\text{sym}} \\ \frac{-j(-1)^{k+l}}{2\pi(k-l)} \left(\mathrm{e}^{j2\pi kt/T_{\text{sym}}} - \mathrm{e}^{j2\pi lt/T_{\text{sym}}}\right) & \text{if } k \neq l \text{ and } -T_{\text{sym}} \leq t < 0 \\ \frac{j(-1)^{k+l}}{2\pi(k-l)} \left(\mathrm{e}^{j2\pi kt/T_{\text{sym}}} - \mathrm{e}^{j2\pi lt/T_{\text{sym}}}\right) & \text{if } k \neq l \text{ and } 0 \leq t \leq T_{\text{sym}} \\ 0 & \text{otherwise} \end{cases} \tag{3.18}$$

The magnitude of this function is illustrated in Figure 3.1. It is observed that for equal subcarrier numbers, the shape of the CCF's magnitude is triangular in the interval $[-T_{\text{sym}}, +T_{\text{sym}}]$. The consequence is that for this subcarrier, the contribution of an overlapping symbol to the received modulation factor rises linearly with increasing overlap. Figure 3.1 also shows that the interference from equal subcarrier numbers is larger than from any other subcarrier.

The CCF of the frequency-domain representation is

$$\gamma_{S_{\text{base},k},S_{\text{base},l}}(\omega) = \int_{-\infty}^{+\infty} S_{\text{base},k}(\nu)\,\overline{S_{\text{base},l}(\nu - \omega)}\,\mathrm{d}\nu \tag{3.19}$$

Define $Z_{\text{base},l}(\omega) = \overline{S_{\text{base},l}(-\omega)}$ so that $z_{\text{base},l}(t) = \overline{s_{\text{base},l}(t)}$. Now this can be written as

$$\begin{aligned} \gamma_{S_{\text{base},k},S_{\text{base},l}}(\omega) &= \int_{-\infty}^{+\infty} S_{\text{base},k}(\nu)\,Z_{\text{base},l}(\omega - \nu)\,\mathrm{d}\nu \\ &= \left(S_{\text{base},k} * Z_{\text{base},l}\right)(\omega) \end{aligned} \tag{3.20}$$

where $*$ denotes convolution. By application of the frequency-domain convolution theorem, this becomes

$$\gamma_{S_{\text{base},k},S_{\text{base},l}}(\omega) = \mathcal{F}\Big\{s_{\text{base},k}(t)\,z_{\text{base},l}(t)\Big\} = \mathcal{F}\Big\{s_{\text{base},k}(t)\,\overline{s_{\text{base},l}(t)}\Big\} \tag{3.21}$$

It holds that $s_{\text{base},-k}(t) = \overline{s_{\text{base},k}(t)}$ and $s_{\text{base},k}(t)\, s_{\text{base},l}(t) = s_{\text{base},k+l}(t) \,/\, \sqrt{T_{\text{sym}}}$ for the OFDM basis signals, simplifying the above to

$$\gamma_{S_{\text{base},k},S_{\text{base},l}}(\omega) = \frac{1}{\sqrt{T_{\text{sym}}}} S_{\text{base},k-l}(\omega) \tag{3.22}$$

So the CCF of the Fourier transformed basis signals k and l is equal to the Fourier transformed basis signal $(k-l)$, which is sinc-shaped.

3.2.2 CCFs of Hermite basis signals

For the basis signals formed by Hermite functions, use the definition

$$s_{\text{base},k}(t) = h_k(t) \tag{3.23}$$

Recall from theory the FrFT over angle α of Hermite k, giving

$$S_{\text{base},k,\alpha}(u) = \mathrm{e}^{-jk\alpha}\, h_k(u) \tag{3.24}$$

The CCF of the Hermite basis signals in the time-domain is

$$\gamma_{s_{\text{base},k},s_{\text{base},l}}(t) = \gamma_{h_k,h_l}(t) = \int\limits_{-\infty}^{+\infty} h_k(\tau)\, h_l(\tau - t)\, \mathrm{d}\tau \tag{3.25}$$

Notice the absence of the conjugation because Hermites are real-valued functions. The CCF of the fractional-Fourier-transformed basis signals can be derived to be a phase-rotated version of the basis signals' time-domain CCF:

$$\begin{aligned}
\gamma_{S_{\text{base},k,\alpha},S_{\text{base},l,\alpha}}(u) &= \int\limits_{-\infty}^{+\infty} S_{\text{base},k,\alpha}(v)\, \overline{S_{\text{base},k,\alpha}(v-u)}\, \mathrm{d}v \\
&= \int\limits_{-\infty}^{+\infty} \mathrm{e}^{-jk\alpha}\, h_k(v)\, \overline{\mathrm{e}^{-jl\alpha}\, h_l(v-u)}\, \mathrm{d}v \\
&= \mathrm{e}^{-jk\alpha}\, \overline{\mathrm{e}^{-jl\alpha}} \int\limits_{-\infty}^{+\infty} h_k(v)\, \overline{h_l(v-u)}\, \mathrm{d}v \\
&= \mathrm{e}^{j(l-k)\alpha}\, \gamma_{h_k,h_l}(u)
\end{aligned} \tag{3.26}$$

This obviously relates to the fact that Hermites are eigenfunctions of the Fourier transform. For the normal Fourier transformed basis signals $\alpha = \pi/2$, so

$$\gamma_{S_{\text{base},k},S_{\text{base},l}}(\omega) = (-j)^{k-l}\, \gamma_{h_k,h_l}(\omega) \tag{3.27}$$

It is well known and easily derived that the auto-correlation function (ACF) of a Gaussian function, and so $\gamma_{h_0}(t)$, is another Gaussian function. But the ACFs and CCFs of Hermite functions of higher degrees are not trivial.

Table 3.1 gives $\gamma_{h_k,h_l}(t)$ for $k, l \in \{0, \ldots, 3\}$. They were found using the software package MAPLESOFT MAPLE . An analytical derivation is beyond the scope of this thesis. Figure 3.2 shows plots of some of the CCFs.

Some observations can be made by looking at the table: *1*) each entry is a polynomial of degree $k+l$, multiplied with a Gaussian window; *2*) each polynomial contains either even or odd order terms, but never both; *3*) polynomials for $k = 0$ or $l = 0$ consist of only one term and some others (e.g. for $k = 1$ and $l = 3$) lack one term; and *4*) all entries with odd polynomial degree change sign if the table is transposed (i.e. k and l are interchanged). The latter is equivalent to t changing sign if the table is transposed, because these polynomials contain only odd-order terms.

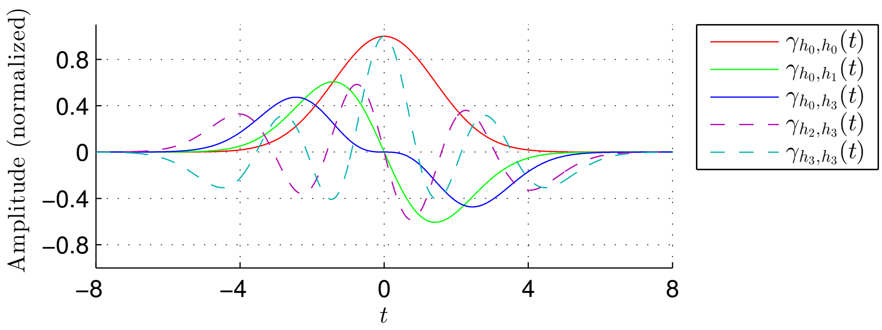

Figure 3.2: *A few CCFs of Hermite functions. The CCF of the two Gaussians is another Gaussian.*

$k \backslash l$	0	1	2	3
0	$e^{-t^2/4}$	$-\frac{\sqrt{2}}{2}t\,e^{-t^2/4}$	$\frac{\sqrt{2}}{4}t^2\,e^{-t^2/4}$	$-\frac{\sqrt{3}}{12}t^3\,e^{-t^2/4}$
1	$\frac{\sqrt{2}}{2}t\,e^{-t^2/4}$	$-\frac{1}{2}(t^2-2)\,e^{-t^2/4}$	$\frac{1}{4}(t^3-4t)\,e^{-t^2/4}$	$-\frac{\sqrt{6}}{24}(t^4-6t^2)\,e^{-t^2/4}$
2	$\frac{\sqrt{2}}{4}t^2\,e^{-t^2/4}$	$-\frac{1}{4}(t^3-4t)\,e^{-t^2/4}$	$\frac{1}{8}(t^4-8t^2+8)\,e^{-t^2/4}$	$-\frac{\sqrt{6}}{48}(t^5-12t^3+24t)\,e^{-t^2/4}$
3	$\frac{\sqrt{3}}{12}t^3\,e^{-t^2/4}$	$-\frac{\sqrt{6}}{24}(t^4-6t^2)\,e^{-t^2/4}$	$\frac{\sqrt{6}}{48}(t^5-12t^3+24t)\,e^{-t^2/4}$	$-\frac{1}{48}(t^6-18t^4+72t^2+48)\,e^{-t^2/4}$

Table 3.1: *CCFs of k^{th}-order with l^{th}-order Hermites : $\gamma_{h_k,h_l}(t)$*

The first observation is interesting because Hermite functions are polynomials multiplied by a Gaussian window as well. Moreover, the second observation also applies to Hermites. These similarities give rise to the question whether the CCFs actually are Hermite functions, which is already the case for $h_0(t)$. The third observation rules out pure Hermite functions but not linear combinations of Hermites. A currently unpublished paper by Korevaar [26] shows that they are indeed linear combinations of Hermites with a maximum degree of $k + l$. The paper presents closed-form expressions for the CCFs, that are not included here.

3.3 The effect of ISI on the BER

In the previous sections the relation between symbol time-frequency placement and impairment of received modulation factors due to ISI was investigated. It was observed that a received modulation factor is the weighted sum of transmitted modulation factors. If the symbol that takes interference and the symbols that cause interference are positioned at either the same time or the same frequency, the weights are found from the CCFs of the basis signals' time-domain or frequency-domain representations, respectively.

Assume the transmitted and received modulation factors are stochastic variables, with the former having a discrete uniform distribution. Hypothetically, if the weights of the sum all have the same value (i.e. the CCFs of the basis signals are equal and constant), then the received modulation factor's probability distribution is approximately Gaussian, by virtue of the central limit theorem (assuming an infinite number of symbols). Hence, in this case ISI manifests itself as an AWGN source and the bit-error probability can be calculated by using Equation 2.16. Obviously, the CCF is in general not constant-valued, which is also observed in the previous section for OFDM and Hermite basis signals. The distribution of the received modulation factor is therefore not easily found with the central limit theorem and it is not necessarily Gaussian.

However, interference can often be considered as a noise source [38]. Some quick calculations on a few simple cases were done during the course of this thesis, with the assumption that the interference source behaves as AWGN. The variance of the interference source relates to the SIR and was used to determine bit-error probability with Equation 2.16. Results of these calculations showed that the bit-error probability is approximated surprisingly well in these cases. However, details of the calculations and exact results will not be presented in this thesis. With regard to calculating BER because of ISI, we conclude that numerical evaluation of the derived equations would be cumbersome. Nevertheless, the derived equations provide insight in the manifestation of ISI in a Hermite-based communication system.

3.4 On the width of Hermite signals

Because the efficiency of spectrum utilization of interest in this thesis, the bandwidth is an important property of the employed (Hermite) signals. However, different definitions are generally in use, of which we will survey a few for practical applicability. Molisch [33] gives three bandwidth definitions:

- Noise bandwidth: "the bandwidth of a system with a rectangular transfer function $|H_{\text{rect}}(f)|$ (and identical peak amplitude $\max(|H(f)|)$ that receives as much noise as the system under consideration."
- 3-dB Bandwidth: "the bandwidth at which $|H(f)|^2$ has decreased to a value that is 3dB below its maximum value."
- 90% Energy bandwidth: "the bandwidth that contains 90% of total emitted energy"

The noise bandwidth applies primarily to systems and is therefore not considered further. The 3-dB bandwidth and 90% energy bandwidth definitions can be generalized to x-dB and y% energy bandwidths, respectively. We refer to the x-dB bandwidth as a magnitude-based bandwidth and expand the above definition by stating that nowhere outside this bandwidth, the signal's spectrum is allowed to exceed the specified level. This avoids confusion about the bandwidth of a signal with e.g. a sinc-shaped spectrum.

Additionally, in relation to the Heisenberg uncertainty principle, the *time spread* T and *frequency spread* Ω of a function $f(t)$ are defined as [28]

$$T^2 \triangleq \frac{\int_{-\infty}^{+\infty} (t-t_0)^2 |f(t)|^2 \, \mathrm{d}t}{\int_{-\infty}^{+\infty} |f(t)|^2 \, \mathrm{d}t} \tag{3.28a}$$

$$\Omega^2 \triangleq \frac{\int_{-\infty}^{+\infty} (\omega-\omega_0)^2 |F(\omega)|^2 \, \mathrm{d}\omega}{\int_{-\infty}^{+\infty} |F(\omega)|^2 \, \mathrm{d}\omega} \tag{3.28b}$$

The uncertainty product is $\Omega T \geq \frac{1}{2}$ for *any* $f(t)$, t_0 and ω_0. Equality is obtained only if $f(t)$ is Gaussian and t_0 and ω_0 are the center points of $|f(t)|^2$ and $|F(\omega)|^2$, respectively [28]. It is known that this product is $\Omega T = \frac{1}{2} + n$ for the n^{th}-order Hermite function [23] and this is the criterion that is used when they are referred to as time-frequency localized functions. The frequency spread can be used as a measure of signal bandwidth.

In principle, the considered bandwidth definitions (magnitude-based, energy-based and 'spread') are all applicable in the time domain as well. This is especially relevant with regard to Hermite functions, because they show similar behavior in both domains.

Different width values can be ascribed to the same signal by different definitions, which is illustrated in Figure 3.3. This figure clearly shows that the 'spread' of a signal does not guarantee that out-of-band emissions are below a certain level, which is important in a multi-user situation. Therefore, this bandwidth definition is not practically applicable in this case. In order to comply with regulations on unlicensed use of white space given by the FCC, a 60-dB bandwidth measure is of interest [23].

Figure 3.4 shows the (time- or band-) widths of the first 32 Hermite functions, using the 'spread', 99%-energy, 3-dB magnitude and 60-dB magnitude definitions. It seems that the difference between the 'spread' and the other width measures grows larger for higher function degree. Clearly, the 60-dB bandwidth attributes the largest width to the signals.

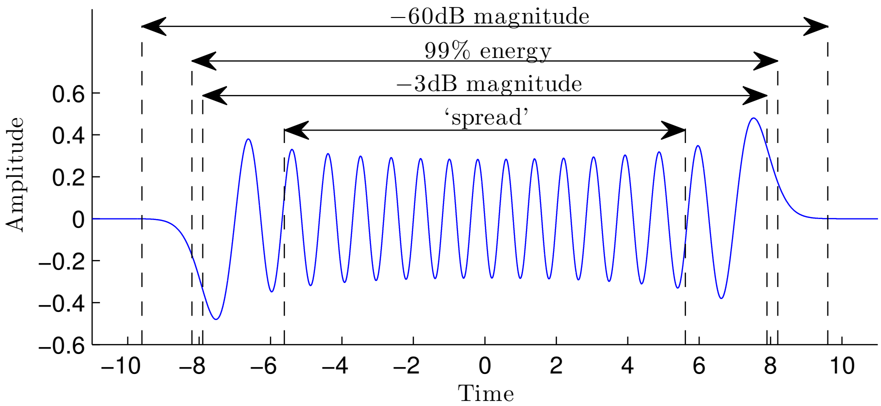

Figure 3.3: *Different width indications for Hermite of degree 31. The width indications also apply to the frequency-domain representation.*

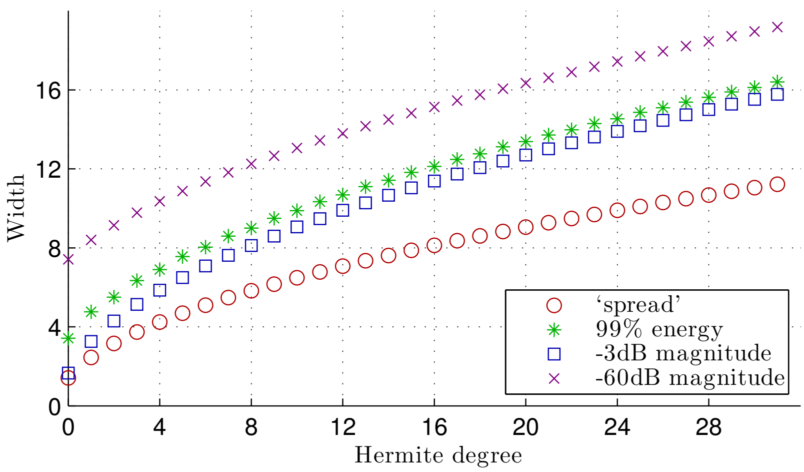

Figure 3.4: *Different width indications for the first 32 Hermites. The width indications apply to both the time domain and the frequency domain.*

3.5 Time-frequency efficiency

The efficiency at which the spectrum is used can be related to the theoretical limit found by Shannon [41]. This limit on the number of modulation degrees of freedom in a given time-frequency area is two per second-Hertz. Consider an arbitrary (rectangular) area in time-frequency of bandwidth BW and duration T. The area contains N_{sym} symbols that consist of N_{c} subcarriers and each subcarrier provides two degrees of modulation freedom. We define the average time-frequency density as

$$\rho \triangleq \frac{2 \cdot N_{\mathrm{sym}} \cdot N_{\mathrm{c}}}{T \cdot BW} \qquad \text{[degrees of freedom/s/Hz]} \tag{3.29}$$

where it is assumed that all symbols are fully contained by the observed area. If this is not the case, the density is approximated if the time-frequency area and the corresponding number of symbols are large. The efficiency or time-frequency density relative to the theoretical limit is now defined as

$$\eta \triangleq \frac{\rho}{2} \tag{3.30}$$

where the 2 comes from the theoretical limit and therefore $0 \leq \eta \leq 1$. Its inverse could be called the inefficiency, but a more suitable name would be the relative time-frequency usage. Hence, this is

$$\zeta \triangleq \frac{1}{\eta} = \frac{T \cdot BW}{N_{\mathrm{sym}} \cdot N_{\mathrm{c}}} \tag{3.31}$$

where it is assumed that $\eta > 0$, i.e. at least one symbol is transferred. Recall the symbol densities of the rectangular and hexagonal symbol distributions from section 2.10 and combine them with Equation 3.31 to relate the relative time-frequency usage to the distance D of one symbol to its nearest neighbor:

$$\zeta_{\mathrm{rect}} = \frac{D^2}{2\pi N_{\mathrm{c}}} \tag{3.32}$$

$$\zeta_{\mathrm{hex}} = \frac{\sqrt{3}D^2}{4\pi N_{\mathrm{c}}} \tag{3.33}$$

In the one-dimensional symbol distributions (section 2.10), the symbols are positioned in time-frequency on a straight line. The average symbol length along this line is naturally well-defined when the number of symbols is large, because it approximates the (average) symbol distance. However, to indicate time-frequency usage in these cases, the symbol width in the direction perpendicular to this line requires an explicit choice. The time-frequency usage is in this case expressed by

$$\zeta_{\mathrm{1d},W} = \frac{D \cdot W}{2\pi N_{\mathrm{c}}} \tag{3.34}$$

where W is the width that is found by applying one of the width definitions. Alternatively, the time-frequency usage can be indicated by assuming that widths are equal in both dimensions:

$$\zeta_{\mathrm{1d}} = \frac{D^2}{2\pi N_{\mathrm{c}}} \tag{3.35}$$

Notice that the time-frequency usage is considered equal to a rectangular grid with the same symbol spacing, as illustrated in Figure 3.5.

When considering the practical application of a Hermite system as an unlicensed user transmitting in a white space, the 60-dB bandwidth is used with Equation 3.34. However, when we are investigating manifestation of ISI in a spectrum filled with Hermite-based symbols, it is interesting to observe ISI in one direction of the time-frequency plane. By comparing the results with two-dimensional grids, the effects of additional ISI can be studied. In this situation, Equation 3.35 is useful, because it allows comparison of points at which certain phenomena are observed.

The relative time-frequency usage provides a convenient measure for the comparison of different transmission schemes, such as the OFDM and Hermite-based communications systems.

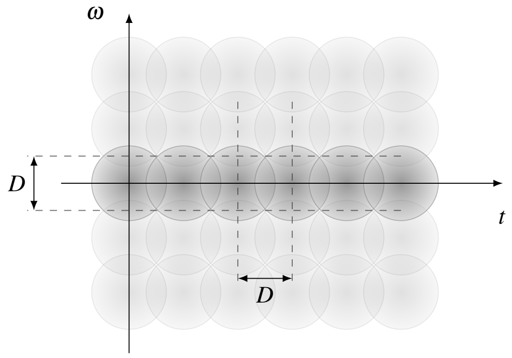

Figure 3.5: *Time-frequency illustration of a one-dimensional symbol grid for comparison of ISI manifestation with two-dimensional grids. Lighter colored symbols are drawn for reference only.*

3.6 Criterion on BER

The BER is a common measure for the quality of a digital connection. Distortions of the transmitted signal, e.g. by channel effects or interference, often result in an impairment of this value.

Many situations cause at least a few errors in the received data. At the cost of some added redundancy in transmitted data, these errors can be corrected with the use of coding schemes, such as Turbo or Viterbi coding. However, error correction has its limits regarding the amount of errors that can be corrected: if the received data contains too many errors, the decoder is no longer able to identify and correct (all of) them. Hence, the decoder shows a limit in its error-correcting capacity, sometimes referred to as the quality limit [43] of the decoder, which is expressed as a value for the BER of the data that enters the decoder. For Turbo and Viterbi decoders using coding rates of 1/3 or 1/2, the quality limit lies somewhere between 0.01 and 0.18 [43].

Part of this thesis' goal is to maximize the Hermite system's symbol density while keeping the BER within limits. The criterion on the BER is chosen to be an order of magnitude smaller than the worst-case value of the decoders' quality limits that were just mentioned. This is BER $\leq 10^{-3}$. For any given time-frequency symbol distribution, the density that still satisfies this criterion will be called the *pivotal (symbol) density.* Similarly, the corresponding relative time-frequency usage will be called the *pivotal time-frequency usage*, denoted by ζ_p.

This chapter has given a (mathematical) analysis of ISI manifestation, in particular considering Hermite-based communication. In the cases of purely time- or frequency-directed ISI, it is observed that the CCFs of the basis signals are useful for prediction of ISI effects. The CCFs for OFDM basis signals were derived, but those of Hermite functions proved to be too complex to derive manually within the scope of this thesis. However, it is shown that CCFs of Hermites and those of fractional-Fourier-transformed Hermites differ only by a rotation in the complex plane, which is a consequence of the fact that Hermites are eigenfunctions of the FrFT. A few CCFs of Hermites were found with the aid of computer software and it was concluded that each can be written as a linear combination of multiple Hermite functions. Prediction of BER impairment due to ISI is not fully achieved, because (numerical) evaluation of the derived equations is very extensive. However, the developed (theoretical) insight in ISI manifestation will provide synergy with simulations and measurements.

Relative time-frequency usage is presented as a convenient measure for the comparison of OFDM and Hermite-based systems' spectral efficiencies. We have linked this measure with the time-frequency symbol distributions that were presented in the previous chapter. Lastly, the criterion on BER as a reference point for transmission quality is specified as BER $\leq 10^{-3}$.

The next chapter will shed some light on the practical side of the experiments for this thesis.

Chapter 4

Experiment setup

The main goal of the current chapter is to give information that eases reproduction of simulations and measurements. Furthermore, the information in this chapter may prove useful for others planning similar experiments.

Therefore, the experimental setup and the used tools are discussed. Assumptions that are made are expressed explicitly. Also a few issues with the setup and the employed solutions are treated.

The key tools in the setup are

- A personal computer (PC) running Matlab software, used for simulations and off-line processing for real-world measurements
- Ettus Research Universal Software Radio Peripheral (USRP), the RF front-end for real-world measurements

Simulations are performed completely in Matlab. Performing all relevant signal processing in Matlab scripts keeps the code portable and provides access to the large amount of features contained in this software package. Because of the widespread use of Matlab, it is assumed that the reader has sufficient knowledge thereof and knows how to use its documentation, so we will not elaborate on this.

When performing measurements using a physical channel, the USRP hardware provides the access thereto and some "glue" software is used between the hardware and Matlab (described in section 4.3). Measurements on the real-world channel are performed with the use of a USRP hardware platform. Although this platform has a reasonably large user base, it is not assumed to be known to the reader. Because its documentation seems fragmented, we will introduce its main features and discuss properties that are relevant to our experiments in section 4.2.

Figure 4.1 shows the flow of signals for physical and simulated channels in the measurement setup.

The "Source" nodes provide random binary data to work with. Processing of the binary data to create the transmit signal, consisting of raw baseband samples, is illustratively accomodated in the "Mod" (modulation) node (the inputs of the basis signals, e.g. sinusoids or Hermite functions, are explicitly shown).

The parts indicated with a gray dashed rectangle are considered "the channel". For the physical channel setup, the USRP hardware is included as a part of it. Propagation delay in the received signal, caused by the physical channel and USRP, is corrected by the "Sync" (synchronization) node, using the transmitted signal as a reference. Details of this node are discussed in section 4.4.

The simulated channel corresponds to an AWGN channel model at baseband with noise characteristics similar to the physical channel. As propagation delay is not modeled in simulation, no correction for it is needed.

Recovering binary data from the received baseband signal is performed in the "Demod" (demodulation) node and the "Sink" illustrates the ultimate consumer of the received data. Source data and received data are compared to calculate the BER.

The transmitting and receiving USRPs can be the same device, provided it can operate in full duplex and transmitter-receiver crosstalk is negligible. Our experiments were performed by using a single device in full duplex.

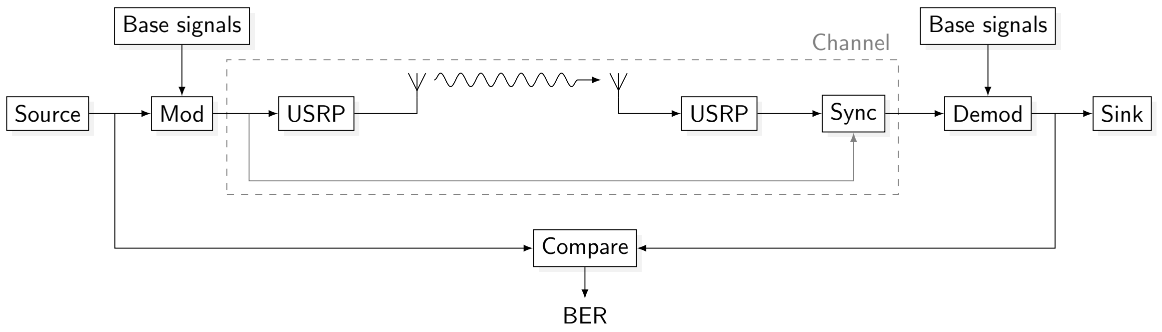

(a) *Physical channel*

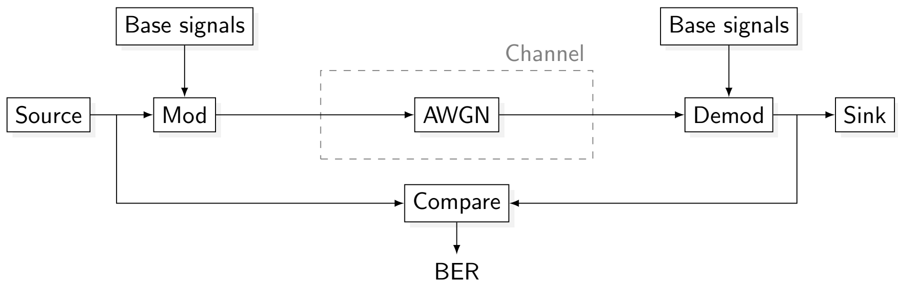

(b) *Simulated channel*

Figure 4.1: *Signal flow of measurement setups*

4.1 Testing environment and assumptions

The experiments take place in an office room at the University of Twente.The room is about 4m wide and 6m long. At about 1/3 of the length and 1/3 of the width, the USRP setup is placed at a height of approximately 80cm on top of a table.

The antennas that we use are the VERT2450 omnidirectional antennas that are available at Ettus Research for use with USRP devices. They are mounted at the front connectors of the USRP, pointing straight up. This results in a spacing between transmit and receive antenna of around 2–3cm.

The physical channel thus formed is assumed to have the following properties:

- Unobstructed, strong LOS path for the RF waves
- Significantly attenuated reflections (w.r.t. LOS)
- Noise is introduced by analog components and the environment

Because of these properties, we assume the channel exhibits a dominant AWGN behavior with any interferers considered part of the noise, no significant multi-path effects, no Doppler shifts and a flat frequency response. Although not a realistic situation for commonly used systems such as WLAN, it is desirable because we intend to use the physical channel to verify results from a simulated AWGN channel.

Furthermore, we make the following assumptions regarding the total system:

- Digital processing is oversampled such that the system approximates the time-continuous case
- Enough amplitude resolution to neglect quantization effects
- Transmitter and receiver LOs are synchronized (i.e. average frequencies are equal)
- Propagation delay is sufficiently compensated by removing the average delay and phase rotation at baseband (see section 4.4)
- Intentional time shifts are an integer multiple of the sample interval

Figure 4.2: *The Ettus Research USRP N210, used for our measurements*

The sample rate is chosen as large as possible and the parameters of the transmitting system are chosen such, that the occupied bandwidth is small enough for the oversampling assumption to hold. For an OFDM system, this means choosing appropriate symbol duration and number of subcarriers, whereas in a Hermite-based system, the time dilation and number of subcarriers are of major importance.

The synchronization of LOs is provided by the USRP hardware.

Fractional delay filters are normally needed when sampled signals are shifted in time by a non-integer multiple of the sample interval [24]. However, to avoid these filters, we round any used delays to the nearest integer number of samples. When possible, we choose to use delay values that do not need rounding and are still consistent with other values used in the system. For other situations, the rounding may introduce inaccuracies, but we assume these are negligible.

The following characteristic parameters are chosen in general:

- Main carrier frequency in 2.45GHz ISM band
- Sample rate $F_\mathrm{S} = 10\mathrm{MS/s}$ for baseband signals
- Synchronized clock signals and LOs of transmitter and receiver
- Gray-coded bit-to-constellation mappings (according to [21, sec. 18.3.5.8])
- No error correction by redundancy (uncoded)
- QPSK modulation
- Output scaling factor $\sigma_\mathrm{A} = \frac{1}{24}$
- Number of transmitted bits $\geq 2^{14}$ per subcarrier

Digitally represented sample values accepted by the USRP are limited, separately for real and imaginary parts, to the range $[-1, +1]$ (corresponding to the digital-to-analog converter (DAC) output swing). To avoid clipping in the USRP hardware, the output values are scaled before transmission with $\sigma_\mathrm{A} = 1/24$ This value was found by observing the absolute maxima of the transmit signal's real and imaginary parts for the Hermite-based system under different conditions.

To be able to measure small BER values, a large amount of source data is needed, because the smallest observable (non-zero) BER is inversely proportional to the number of bits. Additionaly, the stochastic character of received bit values calls for a large number of trials to obtain accurate values. However, the computational power and storage capacity of the hardware used for the experiments, in conjunction with a wish for reasonable execution times, limits the amount of bits that are transmitted. To have enough resolution and accuracy for the individual subcarriers' BERs, at least 2^{14} bits are used for each subcarrier. This is based on the desired BER of 10^{-3}.

4.2 Ettus Research USRP

The most prominent hardware used for our measurements is the USRP hardware platform for software defined radio (SDR) developed by Ettus Research [13]. This platform provides the interface between (analog) RF signals to or from e.g. antennas and a normal PC running software for baseband

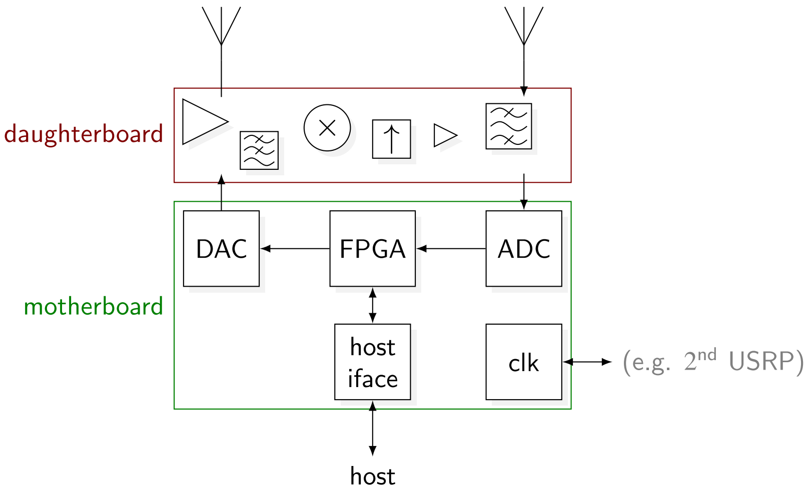

Figure 4.3: *USRP global architecture*

processing. It is intended for e.g. wireless communications prototyping and applications include FM radio transmission or reception, Digital Audio Broadcast (DAB) [36], RF Identification (RFID) [8], Global System for Mobile Communications (GSM) base station [35] and teaching of courses on e.g. radio systems [46]. As a very modular and generic platform, it can be used for many applications.

The USRP hardware and software are open-source, meaning that anyone can obtain the schematics and source codes and use it to tailor the system by modifications or extensions to suit their application. Most notably, part of the field-programmable gate array (FPGA) resources in a USRP is kept available to the user, for additional digital signal processor/processing (DSP) in the hardware. Supporting information is available through the website of Ettus Research [13].

Related to the USRP design project is GNU Radio [18], a software platform for SDR that can be used for flow-based signal-processing prototyping. But both the USRP hardware and GNU Radio can be used in combination with other software and hardware, respectively.

At the moment of writing, there are four categories of USRP devices: the “Bus”, “Networked”, “Embedded” and “X” series. The first provide a Universal Serial Bus (USB) interface to the host PC, such as the original USRP device, the USRP1. Devices of the second category connect to the host by an ethernet interface. Stand-alone-capable devices, that do not require a host PC, are in the “Embedded” series, and devices of the recently-introduced “X” series provide more bandwidth than devices of the other categories. The device used for our experiments is the USRP N210 (see Figure 4.2) of the “Networked” series.

4.2.1 USRP architecture

The USRP devices employ a modular architecture, in which a motherboard contains an interface to a host PC, ADCs and DACs and an FPGA for control and signal processing. The board is equipped with connectors onto which daughterboards with analog processing circuitry can be fitted.

Some daughterboards simply provide a one-to-one connection to the ADCs and DACs. These boards are intended to be used at baseband or low-intermediate frequency (IF), or for applications involving sub-sampling. Other, more complex, boards contain circuitry for analog up- and down-mixing and filtering of signals. These allow fixed or variable (software-controlled) tuning to a specific part of the RF spectrum. The different daughterboards that are available, each provide transmission and reception in a different band within the range of DC upto 6GHz.

Many configurations provide full-duplex operation and boards like the WBX, SBX and CBX, that contain up- and down-mixers, have two separate LOs, enabling the use of different bands for transmission and reception. Many daughterboards provide (additional) analog gain, which can often be controlled by software.

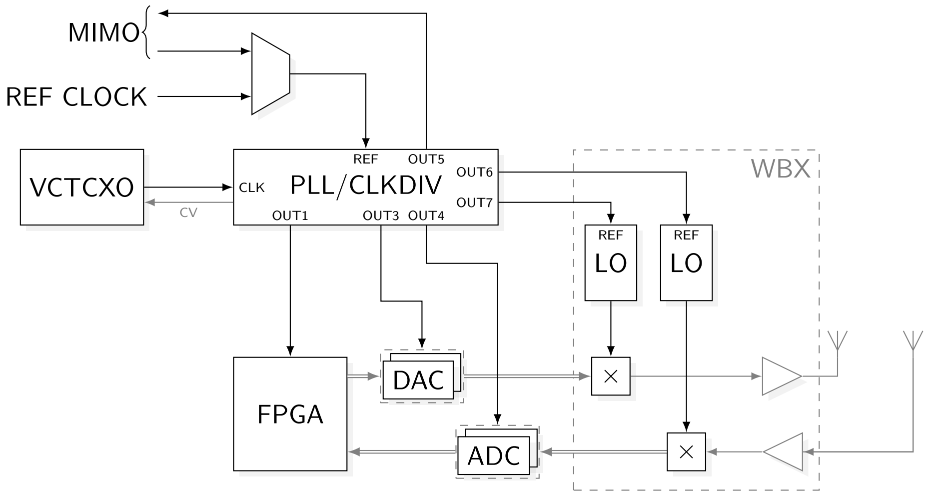

Figure 4.4: *Clock distribution in USRP2+WBX setup (derived from schematics [14] [15])*

The daughterboard used for our measurements is the SBX-board, which can be tuned to frequencies from 400MHz to 4.4GHz with a bandwidth of 40MHz. It has two antenna connectors, enabling separate antennas for transmission and reception and it supports full-duplex operation.

Figure 4.3 illustrates the architecture of the USRP N210 hardware. Two separate transmit chains are on the motherboard, each of which has two DACs, that can be used as separate channels or as I/Q-pair. Similarly, there are two receive chains, with each two ADCs.

Clocks, LOs and synchronization

The clock distribution of a USRP2 device with a WBX daughterboard, which is similar to that of the USRP N210 with SBX, is illustrated in Figure 4.4. The different clocks for motherboard and daughterboard components are derived from a single clock source, ensuring that all LOs and ADCs/DACs can run synchronously. The main clock source can run freely or be synchronized to an external reference. This reference can optionally be another USRP, e.g. when set up for multiple input, multiple output (MIMO) operation, to double the number of (synchronized) transmit and receive channels.

It was observed during early experiments for this thesis, that the received signal was sometimes inverted after re-initializing the USRP. A possible explanation for this is that the LOs of transmitter and receiver individually lock to the main clock, not necessarily at the same time. Hence, the moment that both are locked, the internal clock dividers can have different states, giving a possible phase difference between the output signals. Fortunately, the inversion is easily corrected when processing the baseband signal in software (e.g. the scheme described in section 4.4 can be used for this).

4.2.2 Software interface

Because of the relation between USRP and GNU Radio projects, the two are easily used in conjunction. GNU Radio provides source and sink nodes that represent USRP receiver and transmitter sections, respectively, to use in its flow graphs. On a lower level of abstraction, the USRP Hardware Driver (UHD) provides an interface for software to access the USRP, virtually regardless of the specific model.

4.3 The USRP combined with Matlab scripts

Some extensions for Matlab (and Simulink) exist that enable access to USRP hardware (e.g. [44] and [22]). However, they all seem to have significant limitations and shortcomings that render them less convenient for this thesis' experiments. For example, at the time the experiments were started,

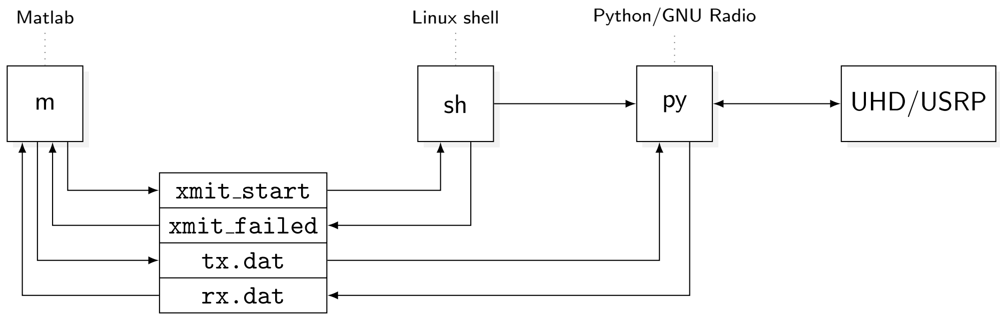

Figure 4.5: *Visualization of the communication between Matlab scripts and the USRP via GNU Radio*

the extension of [44] supported neither full-duplex operation nor non-default daughterboard antenna selection.

Therefore, some custom scripts were written, to use the hardware from within Matlab while keeping sufficient control over the USRP's parameters. In the used method, digital processing is performed off-line, i.e. when the USRP is not actually transfering. This avoids the tight constraints associated with a real-time implementation, providing ample freedom in the complexity of the employed algorithms.

Although the processing capabilities of GNU Radio are barely used, the software is still needed to perform the measurements involving USRP hardware. A GNU Radio script that is run separate from Matlab provides access to the hardware and interacts with the Matlab scripts through files on disk.

Figure 4.5 illustrates the communication between the Matlab scripts and the USRP. Several scripts on the PC are involved in the system:

`air_loopback.m`	Matlab script defining the function `air_loopback()` that may be called from the signal processing script to handle USRP access
`air_loopback.sh`	Linux shell script that handles requests from `air_loopback()` and controls GNU Radio
`air_loopback.py`	GNU Radio Python script describing the signal flow graph between sample files and USRP
`air_loopback_wrapper.py`	Wrapper around GNU Radio script that instantiates it and issues start and stop commands

The `air_loopback()` function takes the baseband samples to transmit as a vector and the sample rate and returns the received baseband samples as a vector. Sample values should be in the range from -1 to $+1$ for both real and imaginary parts.

Before calling `air_loopback()`, the shell script `air_loopback.sh` must be started in a separate process. This script serves to handle control messages from and to `air_loopback()` and calls `air_loopback_wrapper.py` when needed. The control messages are passed as files on disk:

`xmit_start`	Created by `air_loopback()` to indicate transfer start, removed by `air_loopback.sh` when transfer finished. Contents are parameter information.
`xmit_failed`	Created by `air_loopback.sh` when maximum number of transfer attempts exceeded, removed by `air_loopback()` when checked.

The `xmit_start` file contains the command line arguments to pass to `air_loopback_wrapper.py` on execution:

`--samp-rate`	Sample rate (Hz)
`--f-center`	RF center frequency (Hz)
`--duration`	Time duration (s) to execute GNU Radio signal flow graph
`--gain-rx`	Receiver (analog) gain (dB)
`--gain-tx`	Transmitter (analog) gain (dB)

The raw baseband transmit samples given to `air_loopback()` are saved to the file `tx.dat`. After this, the trigger file `xmit_start` is created and the parameters written to it, indicating that the data is ready to be transmitted. A loop is then entered to wait for the removal of the trigger file, i.e. transfer finish.

The separately running shell script periodically checks the existence of the trigger file and if it exists, executes `air_loopback_wrapper.py` with the command line arguments from `xmit_start`. The GNU Radio script transmits the baseband data from file through the USRP and simultaneously saves the received baseband data to the file `rx.dat`. When finished, the shell script removes `xmit_start` to indicate that transfer has finished. On failure, it first creates the file `xmit_failed` to inform the Matlab script.

When `air_loopback()` sees that `xmit_start` is removed, the received baseband samples are loaded from file into memory and passed back to the function's caller.

4.3.1 GNU Radio signal flow graph

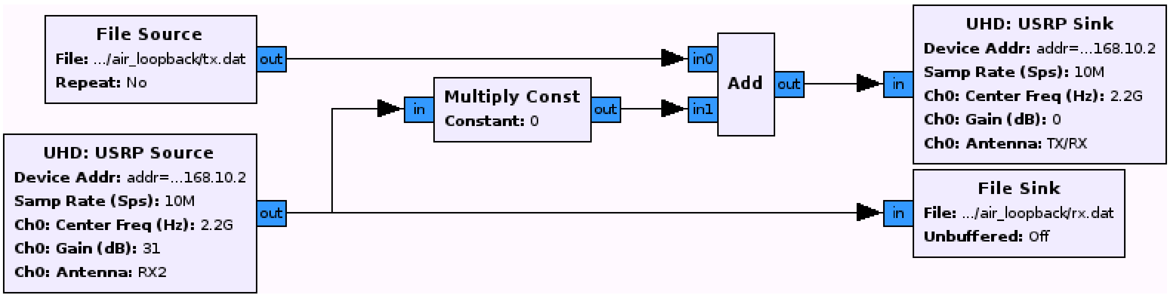

Figure 4.6: *Signal flow graph of GNU Radio script `air_loopback.py`. The dependency between transmit and receive chains ensures that transmission is not started before reception runs.*

The signal flow graph in `air_loopback.py`, created using GNU Radio Companion (the graphical interface for GNU Radio), is shown in Figure 4.6. The transmitting part of the USRP corresponds to the "USRP Sink" in the flow graph and the receiving part is the "USRP Source". Notice the link between transmission and reception paths in the flow graph. Because GNU Radio operates separate paths in its flow graph independently, transmission and reception do not start simultaneously. To make sure the complete transmitted signal is received, the transmit path is made dependent on the receive path in the flow graph. This way, transmission can not start earlier than reception. The addition of the received signal multiplied by a constant zero to the transmit signal does not alter the transmit signal itself.

4.4 Time synchronization

In simulation, the transmit and receive signals have the same start time. When an AWGN channel is simulated, the channel has no influence on temporal properties of the signal, so the first sample of the transmit signal corresponds exactly to the first sample of the receive signal.

Any physical communication channel exhibits a propagation delay. This delay, primarily occurring in the RF signal, manifests itself at baseband as both a time- and phase-shift of the received signal. The following equation models a channel at baseband with (only) this behavior (based on [39]):

$$s_{\mathrm{rx}}(t) = s_{\mathrm{tx}}(t - T_{\mathrm{p}})\mathrm{e}^{j\Phi_{\mathrm{p}}}$$

where T_{p} is the propagation delay and Φ_{p} is the phase rotation due to the propagation delay.

Demodulation using a matched filter, such as described in chapter 2, assumes (perfect) time synchronization between transmitter and receiver. Hence, propagation delay must be undone before demodulation (visualized earlier with the "Sync" node in Figure 4.1a). In order to accomplish this, the values of T_{p} and Φ_{p} must be known.

Ideally, the phase rotation is $\Phi_\mathrm{p} = -j2\pi F_\mathrm{C} T_\mathrm{p}$, where F_C is the main carrier frequency. This suggests that Φ_p can be derived from T_p [39]. However, the phase is not easily calculated from T_p in practice, notably because an accurate value of F_C is not easily obtained.

A way of finding the actual values of T_p and Φ_p is by using cross correlation of the received and transmitted signals and finding the position of the maximum magnitude of the result. This method assumes that channel properties do not change significantly while it is used. Hence,

$$\gamma_{\mathrm{rx,tx}}(\tau) = \int_{-\infty}^{+\infty} s_\mathrm{rx}(t) \cdot \overline{s_\mathrm{tx}(t-\tau)}\, \mathrm{d}\tau \tag{4.1}$$

$$\hat{T}_\mathrm{p} = \operatorname*{argmax}_{\tau} \left|\gamma_{\mathrm{rx,tx}}(\tau)\right| \tag{4.2}$$

$$\hat{\Phi}_\mathrm{p} = \arg\left(\gamma_{\mathrm{rx,tx}}(\hat{T}_\mathrm{p})\right) \tag{4.3}$$

where $\hat{T}_\mathrm{p}$ and $\hat{\Phi}_\mathrm{p}$ are the estimations of T_p and Φ_p, respectively.

An estimation of the transmitted signal is

$$\hat{s}_\mathrm{tx}(t) = s_\mathrm{rx}(t + \hat{T}_\mathrm{p})\mathrm{e}^{-j\hat{\Phi}_\mathrm{p}} \tag{4.4}$$

For implementation, the substitution $\mathrm{e}^{-j\hat{\Phi}_\mathrm{p}} = \left|\gamma_{\mathrm{rx,tx}}(\hat{T}_\mathrm{p})\right|^{-1} \cdot \overline{\gamma_{\mathrm{rx,tx}}(\hat{T}_\mathrm{p})}$ might be convenient.

The described time synchronization method requires that the raw transmitted signal is also available at the receiver (indicated by the gray arrow bypassing the channel in Figure 4.1a). This way no special synchronization techniques like pilot carriers, with their own limitations, are needed. Of course, in a real communication system, the transmitted samples are not known at the receiver, so a different synchronization scheme must be used.

4.5 The use of baseband DC and IF

In practical communication systems, using frequencies close to DC at baseband is often avoided. Otherwise, LO bleedthrough can occur, because baseband DC corresponds to the main carrier frequency at RF. Also, the analog stages in the baseband signal path can easily introduce offsets in voltage or current, interfering with the information at DC (or frequencies close to DC because of offset variations/drift).

In OFDM systems, this problem is commonly mitigated by disabling a number of subcarriers close to baseband DC. Because Hermite functions of different orders do not stack in frequency like the subcarriers in OFDM, the same solution is not suitable for the Hermite-based system. Therefore, the digital baseband signal is translated to a (low) IF (multiplication in the time domain by $\mathrm{e}^{j2\pi F_\mathrm{if} t}$) before conversion to analog. At the receiver, the signal is translated back. The resulting signal at RF is similar to a SSB/single sideband supressed carrier (SSBSC)-modulated carrier.

The scheme requires that the original baseband signal occupies less than half the DAC/ADC bandwidth, because its spectral content must fit between DC and the maximum positive frequency, to avoid problems associated with DC and aliasing. Assuming that the original signal's spectral content is centered at DC, the value of F_if must be at least half the signal bandwidth.

4.6 Noise characteristics estimation

For a fair comparison between simulated- and real-channel results, the noise characteristics of the simulated AWGN channel are set to match with the real channel.

Consider the AWGN channel model of Equation 2.15:

$$s_\mathrm{rx}(t) = \alpha s_\mathrm{tx}(t) + s_\mathrm{n}(t) \tag{4.5}$$

where $s_\mathrm{tx}(t)$ and $s_\mathrm{rx}(t)$ are the transmitted and received signals, respectively, α is the linear gain of the channel and $s_\mathrm{n}(t)$ is the added noise. In order to obtain values for α and N_0, a reference signal is transmitted through the real channel and the received signal is compared with the transmitted signal. The reference signal is a single complex exponential at (baseband) frequency F_{ref} with power $P_{\text{ref,tx}}$. A single harmonic signal is used because its frequency-domain representation consists of a single peak that is easily distinguished from the noise floor.

Analysis of the received signal is performed by means of a discrete Fourier transform (DFT). The frequency of the reference signal is chosen to be exactly in the middle of a DFT bin and its power is calculated from the DFT magnitude of this bin. It is assumed that clock/LO jitter is small enough to keep the reference signal's power sufficiently in this single bin. Furthermore, it is assumed that the noise power within the frequency band represented by the bin is negligible when compared to the received reference signal power $P_{\text{ref,rx}}$. This assumption is valid if $P_{\text{ref,rx}}$ and the number of DFT bins are large.

Because baseband DC is subject to the influences of offset voltages and currents in the analog processing path of the radio hardware, it is often removed from noise analyses. This means that the corresponding DFT bin is discarded. Furthermore, the physical channel (notably including analog circuitry) is never completely linear, so harmonic distortion products are present in the received signal. These distortion products are normally considered part of neither the noise, nor the (reference) signal (consider the definitions of SNR, signal-to-noise and distortion ratio (S/N+D) and total harmonic distortion (THD) in [4]). The powers in the bins that correspond to the distortion products are summed to give the total harmonic distortion power P_{thd}. Note that the same assumptions are made as for the received reference power bin. The sum of the remaining DFT bins' powers is approximately the total received noise power P_{n}.

The two parameters α and N_0 for the AWGN channel model are found by

$$\alpha = \sqrt{\frac{P_{\text{ref,rx}}}{P_{\text{ref,tx}}}} \tag{4.6}$$

$$N_0 = \frac{P_{\text{n}}}{BW} \tag{4.7}$$

where BW is the observed bandwidth, which is equal to the sample rate in case of I/Q sampling.

Measurements were performed using our USRP setup, with $F_{\text{S}} = 10\text{MS/s}$, $P_{\text{ref,tx}} = 1$ and $F_{\text{ref}} = 1.5\text{MHz}$, resulting in

$$\begin{aligned} P_{\text{ref,rx}} &\approx -11.5\text{dB} \\ P_{\text{n}} &\approx -47.1\text{dB} \\ P_{\text{dist}} &\approx -47.2\text{dB} \end{aligned}$$

where the powers are relative to the ADCs' full scale (in GNU Radio and Matlab unitless $[-1, +1]$ for both the I- and the Q-path). From these powers, we calculate

$$\begin{aligned} \alpha &\approx 0.27 \\ N_0 &\approx -117\text{dB} \\ \text{SNR} &\approx 35.6\text{dB} \\ \text{S/N+D} &\approx 32.7\text{dB} \\ \text{THD} &\approx -35.7\text{dB} \end{aligned}$$

This chapter presented the setup that was used for this thesis' experiments. Practical choices and assumptions were presented. As an essential part of the setup, the chosen hardware for experimental radio transmission, the Ettus Research USRP, was described. The coupling between The Mathworks Matlab software and USRP hardware that was presented, was a practical solution but not ideal. The issue of compensating for propagation delay and timing missynchronization between transmitter and receiver was addressed and a pragmatic approach was taken to solve it for this setup. In addition to this, it was observed and noted that the use of low-frequency information-carrying signals at baseband leads to problems and the use of an IF was chosen as a solution. Finally, the attenuation and noise characteristics of the physical channel corresponding to the setup were determined, in order to match simulation and practice.

The next chapter will present results that were obtained with the use of the setup from this chapter.

Chapter 5

Results from simulations and measurements

In this chapter, the effect of ISI on the BER in Hermite-based communication is examined by means of simulations and measurements. The results are linked to the theoretical analyses of chapter 3 to come to a complete picture.

At first, ISI is deliberately limited to a single direction in the time-frequency plane, in order to verify that ISI direction has no influence. These results also show a few characteristic aspects of the system's behavior, such as the dependency on symbol spacing and the error contributions of individual subcarriers. Results are combined with the 60-dB bandwidth definition to show performance when the system operates in spectral white space for its transmission. Then, two-dimensional symbol distributions are brought into play in order to assess spectral efficiency for multi-user situations when the BER is constrained. Lastly, behavior in AWGN channels is examined and noise- and interference-limited performance regimes are identified.

An OFDM system is subjected to similar trials for comparison with the Hermite system. The chapter will conclude with a brief exploration of a system employing the Fourier-Hermite basis signals.

It is important to note that for all simulations that do not include an explicit indication of the noise level, we used $E_\mathrm{b}/N_0 \approx 46$dB, corresponding to the real-channel setup. Pivotal densities are also determined with this noise level.

5.1 Hermite-basis ISI in single-dimension symbol overlap

Simulations of the Hermite-based system with the inherent ISI in one direction (time-directed, frequency-directed or diagonal) were performed, of which Figure 5.1a shows the total BER versus relative time-frequency usage. In all simulated cases the BER decreases in a virtually monotonic fashion when symbols are allowed more area in time-frequency, i.e. symbol spacing is increased and thus ISI reduced.

Each curve stops when no bit errors occur anymore. Because a small amount of white Gaussian noise is added ($E_\mathrm{b}/N_0 \approx 46$dB) in the simulated channel, the theoretical bit-error probability is never completely zero. Hence, if a BER of zero is observed, this is due to the finite number of transmitted bits in the simulations.

In chapter 3, it was stated that, because Hermites are eigenfunctions of the FrFT, ISI should not be influenced by the direction in time-frequency at which it occurs. This is confirmed by the simulations for eight and sixteen subcarriers. However, when a single subcarrier is employed, the results of different directions do not completely match, which is shown with more detail in Figure 5.1b. Most striking is the significantly earlier, sudden drop to zero of the BER in the time-directed case. Simulations without noise do not produce noticably different results, hence the phenomenon is not related to noise. Also, time-truncation of the basis signals (necessary for practical reasons, as stated in subsection 2.8.2) can neither be the cause, because it occurs at points where the Hermites' exponential decay has reduced its effect to be smaller than that of the noise. Another possibility is the influence of limited bandwidth with the chosen sample rate, causing additional errors in the frequency- and

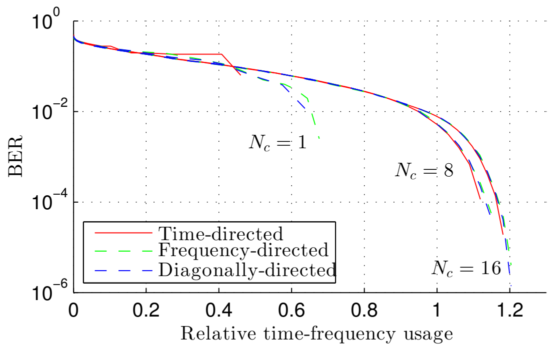

(a) *Total system's BER as a function of time-frequency usage*

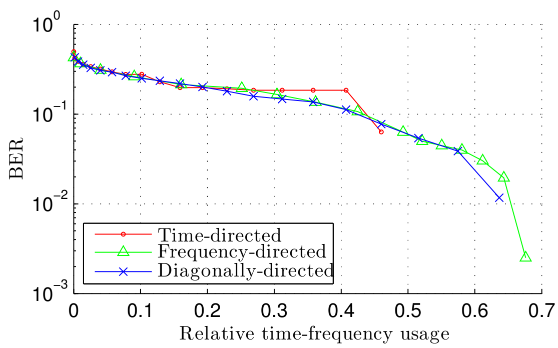

(b) *Same as (a), but showing only $N_c = 1$.*

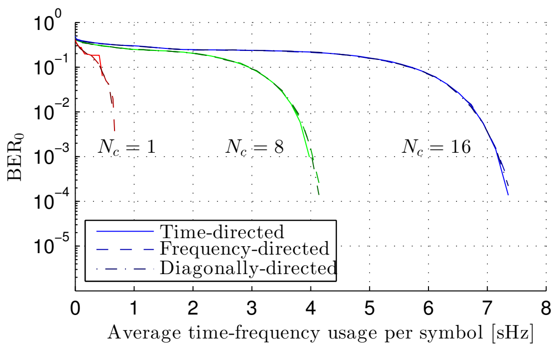

(c) *BER of subcarrier 0 as a function of time-frequency usage per symbol.*

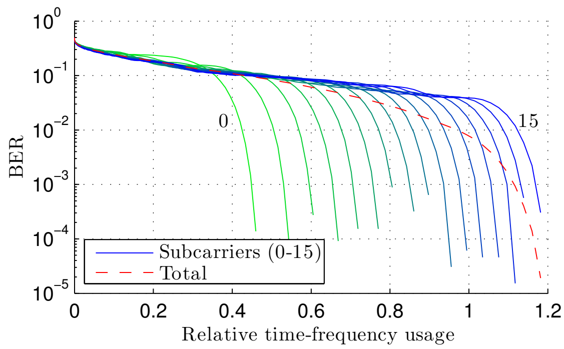

(d) *BER per subcarrier for time-directed ISI with 16 subcarriers. Curve colors from green to blue correspond to subcarriers 0 to 15*

Figure 5.1: *Simulated-channel BER performance of Hermite system due to ISI in one dimension. Time-frequency usage corresponds to Equation 3.35.*

diagonal-directed distributions. Because the bandwidth of the transmitted signal was smaller for the diagonal distribution, the effect should be smaller as well, which is not clearly observable. However, the effect of the sample rate is not examined thoroughly. Hence, it is currently unclear what the cause is.

Regardless of the influence by the direction of ISI, there is a clear effect from the number of subcarriers. Whereas the observed difference between eight and sixteen subcarriers is small, the single-subcarrier system exhibits BER roll-off significantly earlier. This anomaly in the results for a single-carrier system is probably because there are fewer subcarriers to contribute significantly to the interference energy. This is explained in the following text frame.

Behavior of single-carrier Hermite system with one-dimensional symbol grids

Consider a single-carrier (Hermite-based) system that uses BPSK modulation ($A_n \in \{-1, +1\}$) and transmits through an ideal noiseless channel. Source data is a random bit stream with equiprobable bit values. If no interference occurs, the transmitted and received modulation factors are equal. Now assume that two adjacent symbols interfere and each has a contribution of a_1 to the received modulation factor:

$$\hat{A}_n = A_n + a_1(A_{n-1} + A_{n+1}) \tag{5.1}$$

The resulting constellation diagram at the receiver is shown here:

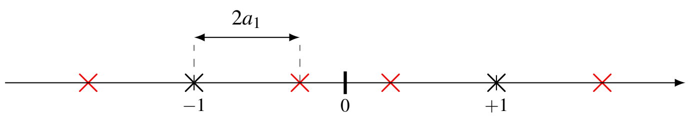

As the symbols are positioned more densely, the value of a_1 increases and the constellation points closest to zero move towards the other side. When $a > 1/2$, these points cross the decision boundary (zero) and errors start to occur. It is easily found that the bit-error probability for this system is either zero or 1/4, depending on symbol density.

Next, we take into account the symbols of one position further, each with a contribution of a_2:

$$\hat{A}_n = A_n + a_1(A_{n-1} + A_{n+1}) + a_2(A_{n-2} + A_{n+2}) \tag{5.2}$$

Assuming $1 > a_1 > a_2$, the received constellation looks like:

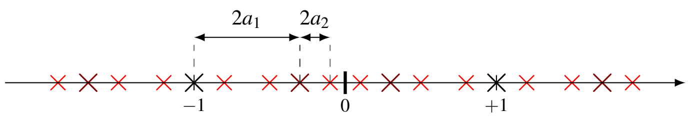

For small a_1 and a_2, no errors occur, but if the density increases, so do a_1 and a_2, causing multiple constellation points to move towards the decision boundary. When $a_1 + a_2$ becomes slightly larger than 1/2, the first points cross the boundary and the bit-error probability is 1/16. As density is raised, the bit-error probability increases in discrete steps, each time a new point crosses the boundary.

Note that, although no errors occur with an ideal channel, noise sensitivity has increased because the interference causes constellation points to be closer to the decision boundary. If the channel introduces AWGN, the discrete steps become less pronounced and a lower bound on the amount of errors appears. As the noise level increases, the relation between density and error probability becomes more smooth and simultaneously the lower bound increases.

Now consider a case in which a multitude of interfering symbols are present. The received modulation factor is now a sum of many terms. The more (strong) interferers there are, the more the total effect resembles AWGN, like the central limit theorem describes. Hence, the BER as a function of symbol density becomes smoother and the gap between zero and the lowest non-zero

Behavior of single-carrier Hermite system with one-dimensional symbol grids (cont)

error rate becomes smaller. If N_c subcarriers are employed, each interfering symbol contributes N_c terms to the sum and similar effects occur.

In our simulations, we have employed QPSK modulation. Higher constellations give more closely spaced decision boundaries and thus the effect of interference is amplified. Furthermore, there are more decision boundaries, causing extra influence on the results.

The values of $a_1, a_2, \ldots$ are the result of the CCFs of the basis signals, like we have shown before. Therefore, the sequence a_p (with $p \in \mathbb{N}$) resembles a sampled version of the basis signal's CCF in the case of a single subcarrier. Hence, in a Hermite system with a single subcarrier, the exponential behavior of the function causes later elements in the sequence to have very small magnitudes. The corresponding symbols thus barely contribute to the received modulation factor and the effect is similar to a low number of interferers. As symbol spacing increases, fewer symbols preserve a significant contribution.

Concluding, the single-carrier Hermite system with one-dimensional ISI behaves differently than the eight- and sixteen-carrier systems because:

- there are few significant interferers,
- the noise level of the channel is low ($E_b/N_0 \approx 46$dB) and
- a low-order constellation (QPSK) is used.

In results that are not shown here, it was observed that for two and four subcarriers, BER roll-off occurs later than for one subcarrier, but earlier than for eight. For increasing number of subcarriers, the cut-off point shifts towards the right in the plot, which fits the explanation in the text frame.

The effect of additional subcarriers on the BER of the Gaussian subcarrier is shown in Figure 5.1c. The horizontal axis of the figure shows the average time-frequency usage per symbol, i.e. $N_c\,\zeta$. Clearly, a larger symbol spacing is needed to keep the BER of subcarrier 0 constant when more subcarriers are used, because of the larger spread of higher order Hermite functions. Time-frequency direction of the interference is of negligible influence, as expected.

The larger time and frequency spread of higher-order Hermites not only causes the interference from these subcarriers *onto* others to increase, but also the interference they receive *from* others. This is demonstrated for $N_c = 16$ in Figure 5.1d. When the relative time-frequency usage increases, the subcarriers' BERs drop sequentially, starting with subcarrier 0, followed by 1, 2 and so on. Interestingly, in the range just before dropping to zero, the BERs show a reduced decrease and absolute values that are higher than other subcarriers (including higher orders). This might be related to the fact that (higher-order) Hermites reach their maximum magnitude just before exponential roll-off.

Using the setup described in chapter 4, measurements were performed to verify simulated-channel results. The results are shown in Figures 5.2a–5.2c, that are the counterparts of Figures 5.1a–5.1d for the real channel. Measurements for the real channel are very consistent with the corresponding simulations. Hence, the real channel seems to behave very similar to the simulated AWGN channel, which is not very surprising given the close spacing of the antennas. Some additional small-scale variations are visible in the BER graphs. These may be due to spurious interference from other transmitters or because of e.g. analog filtering.

From the results, the values for the pivotal time-frequency usage ζ_p are extracted and they are summarized in Table 5.1. These values will generally not be applicable to a real implementation of the system, because equal signal widths in both directions in the time-frequency plane were assumed. Figure 5.3 shows the results for one-dimensional symbol distributions when the transmitted signal's 60-dB width is considered. This figure gives a more realistic indication of the time-frequency usage when the system is an unlicensed user with out-of-band emission restricted to FCC regulations. The pivotal time-frequency usage ζ_p values for this situation are listed in Table 5.2. Although spectral efficiency appears to be low, the system does not exhibit spectral leakage. In this case, 'safety' (avoiding interference) has higher priority than efficiency. However, spectral efficiency increases with the number of subcarriers, providing an opportunity to enhance the performance while staying 'safe'.

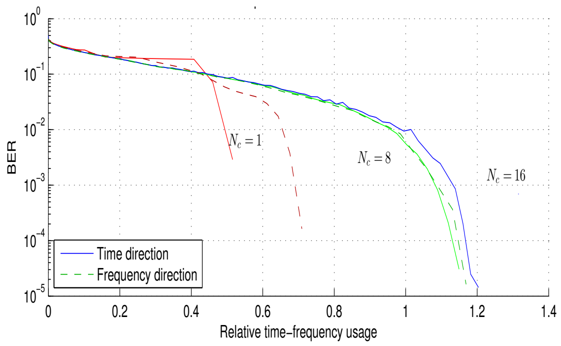

(a) *Total system's BER as a function of time-frequency usage*

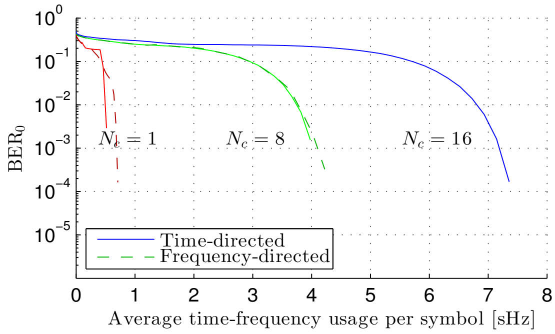

(b) *BER of subcarrier* 0 *as a function of time-frequency usage per symbol.*

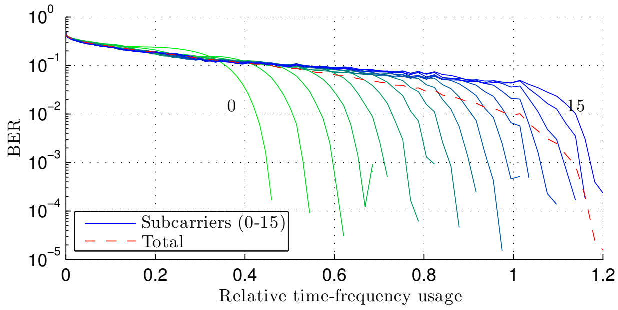

(c) *BER per subcarrier for time-directed ISI with* 16 *subcarriers. Curve colors from green to blue correspond to subcarriers* 0 *to* 15

Figure 5.2: *Real-channel BER performance of Hermite system due to ISI in one dimension. Time-frequency usage corresponds to Equation 3.35.*

	Time-directed		**Frequency-directed**		**Diagonal**
N_c	Simulation	Real	Simulation	Real	Simulation
1	0.52	0.57	0.70	0.70	0.70
8	1.09	1.09	1.09	1.09	1.09
16	1.12	1.14	1.14		1.12

Table 5.1: *Pivotal time-frequency usage of Hermite system for one-dimensional symbol distributions assuming equal symbol width in both directions. The time-frequency usage corresponds to Equation 3.35. The numbers for $N_c = 1$ are explained in the text frame on page 43.*

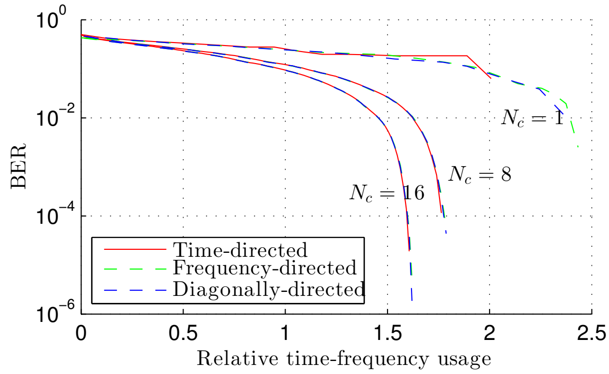

Figure 5.3: *Simulated-channel BER performance of Hermite system due to ISI in one dimension. Time-frequency usage corresponds to Equation 3.34 with* 60*-dB bandwidth.*

	Time-directed		**Frequency-directed**		**Diagonal**
N_c	Simulation	Real	Simulation	Real	Simulation
1	2.13	2.24	2.48	2.48	2.48
8	1.74	1.74	1.74	1.74	1.74
16	1.56	1.58	1.58		1.56

Table 5.2: *Pivotal time-frequency usage of Hermite system for one-dimensional symbol distributions when considering* 60*-dB bandwidth. The time-frequency usage corresponds to Equation 3.34.*

We will see a similar effect in section 5.3, where an explanation is given as well. The maximum realistic spectral efficiency obtained in the simulations with the one-dimensional grids is about 1.28 modulation degrees of freedom per second-Hertz, using sixteen subcarriers.

5.2 ISI in rectangular and hexagonal symbol distributions

Simulations of the Hermite-based system using the rectangular and hexagonal grids provide the resulting total BER performances that are shown in Figure 5.4. The two-dimensional distributions exhibit a higher overall BER than the one-dimensional ones, evidently because each symbol takes interference from multiple directions. The curves for the rectangular and hexagonal distributions are similar when a single subcarrier is used. However, when eight or sixteen subcarriers are employed, the BERs of the hexagonal distribution fall more sharply above $\zeta \approx 0.8$. This results in a lower time-frequency usage of this symbol distribution for the given BER of 10^{-3}, and thus higher spectral efficiency, compared to the rectangular grid.

Table 5.3 gives the extracted values of the pivotal time-frequency usage ζ_p for rectangular and

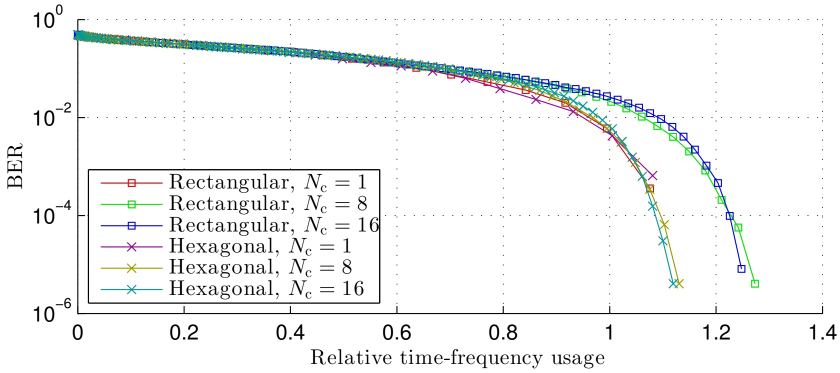

Figure 5.4: *Simulated Hermite system's BER performance for two-dimensional symbol distributions.*

N_c	**Rectangular** Simulation	**Hexagonal** Simulation
1	1.08	1.08
8	1.18	1.08
16	1.20	1.06

Table 5.3: *Pivotal time-frequency usage of Hermite system for 2-dimensional time-frequency symbol distributions.*

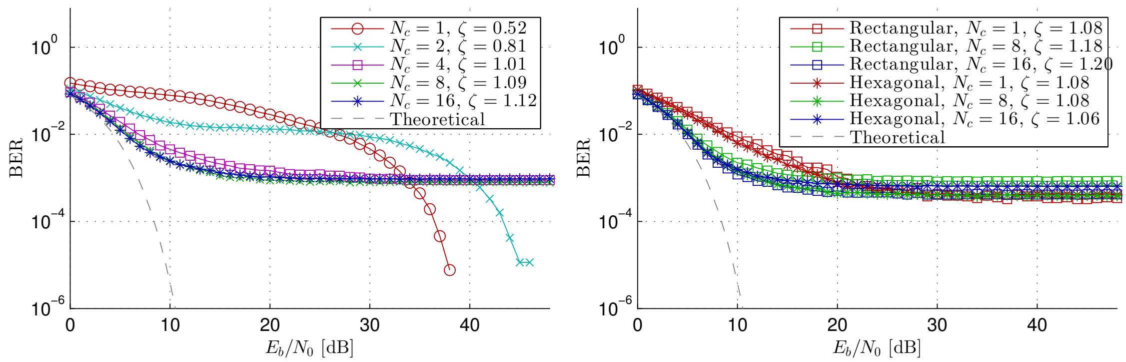

(a) *One-dimensional symbol distribution* **(b)** *Rectangular and hexagonal distributions*

Figure 5.5: *Simulated noise influence on Hermite system's BER performance for different symbol distributions and numbers of subcarriers, with pivotal density.*

hexagonal symbol distributions. There is little deviation between the values for the rectangular and hexagonal distributions, but the latter has a slight overall advantage.

It is shown that communications using Hermite functions as basis signals can be performed with a spectral efficiency of about 1.85 degrees of freedom per sHz when the total BER is limited to 10^{-3}. However, time dispersion and frequency dispersion are small for the real-channel measurements and absent for simulations. Channel noise (AWGN) is small for both simulations and real-channel measurements. Furthermore, in practical applications, the effective data throughput is reduced because of the necessity for error-correction codes.

5.3 AWGN performance

It is relevant to investigate under what circumstances the system performance is limited predominantly by the inherent ISI or by noise in AWGN channels. This helps to analyze the impact of the non-orthogonality of time-frequency shifted Hermite sets.

For a one-dimensional symbol distribution, the simulated BER as a function of signal-to-noise ratio per bit (E_b/N_0) is shown in Figure 5.5a for various numbers subcarriers and the corresponding pivotal time-frequency usage values. For reference, the theoretical performance of a system without ISI in an AWGN channel, is shown as well. Because of the earlier-observed difference between time- and frequency-directed distributions, both are shown. None of these systems come very close to the theoretical curve. Naturally, ISI is the dominant cause for errors when E_b/N_0 is high.

A salient difference in the shape of the curves occurs between systems with fewer or more subcarriers. The systems with one and two subcarriers perform very poor in the lower part of the simulated E_b/N_0 range and drop to zero BER in the upper part. However, the other systems perform considerably better for lower E_b/N_0 and approach a lower-bound around BER $\approx 10^{-3}$ (likely related to the used BER criterion) as E_b/N_0 increases. A probable cause lies in the shape of the received modulation factors' probability density functions (PDFs). This could also relate to the explanation given in the text frame on page 43. However, a more detailed explanation is currently not found.

The results of Figure 5.5b show that for the rectangular and hexagonal symbol distributions, the curves behave similar to the one-dimensional cases that use more subcarriers. A possible explana-

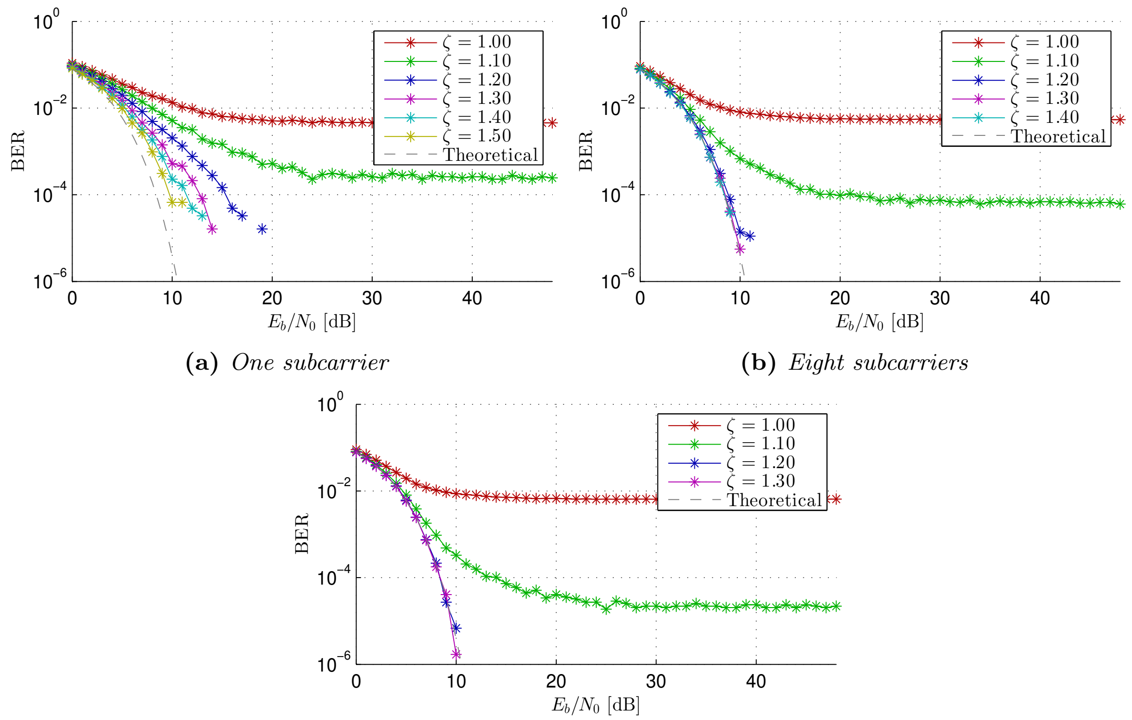

(a) *One subcarrier* **(b)** *Eight subcarriers*

(c) *Sixteen subcarriers*

Figure 5.6: *Simulated noise influence on Hermite system's BER performance for various symbol densities in hexagonal grid.*

tion for this observation is that the number of symbols closest to one specific symbol is 2 for the one-dimensional symbol distributions, but 4 and 6 for rectangular and hexagonal distributions, respectively. The result is that each symbol takes equally strong interference from multiple directions in time-frequency, with an effect on the received modulation factors' PDFs that is similar to that of multiple subcarriers. This was described in more detail in the text frame on page 43. Figure 5.5b also shows that for single-carrier systems, the curves of two-dimensional distributions have some tendency towards the one-dimensional cases with few subcarriers. The multi-carrier curves more closely follow the theoretical curve for lower E_b/N_0. This is again the effect of a larger number of significant interferers.

The plots in Figure 5.6 show AWGN performance for a system employing the hexagonal symbol distribution with various symbol densities. All three plots show that when symbol spacing is increased, the curve tends more towards the theoretical ideal, which is because ISI is reduced. However, as subcarriers are added, ideal behavior is approached faster with increasing time-frequency usage.

In order to obtain the BER of 10^{-3} in an AWGN channel, the theoretical (non-interference) E_b/N_0 must be at least 6.8dB. Table 5.4 lists the minimum required E_b/N_0 for the Hermite systems,

	E_b/N_0 [dB]		
ζ	$N_c = 1$	$N_c = 8$	$N_c = 16$
1.1	15.9 (+9.1)	9.1 (+2.3)	8.0 (+1.2)
1.2	11.6 (+4.8)	7.1 (+0.3)	6.8 (+0.0)
1.3	9.4 (+2.6)	6.9 (+0.1)	6.8 (+0.0)
1.4	8.7 (+1.9)	6.8 (+0.0)	
1.5	8.0 (+1.2)		

Table 5.4: *Minimum required E_b/N_0 to achieve BER $\leq 10^{-3}$ with Hermite-based transmission in an AWGN channel. Theoretically required value is 6.8dB without interference. The values between parentheses indicate the required additional E_b/N_0.*

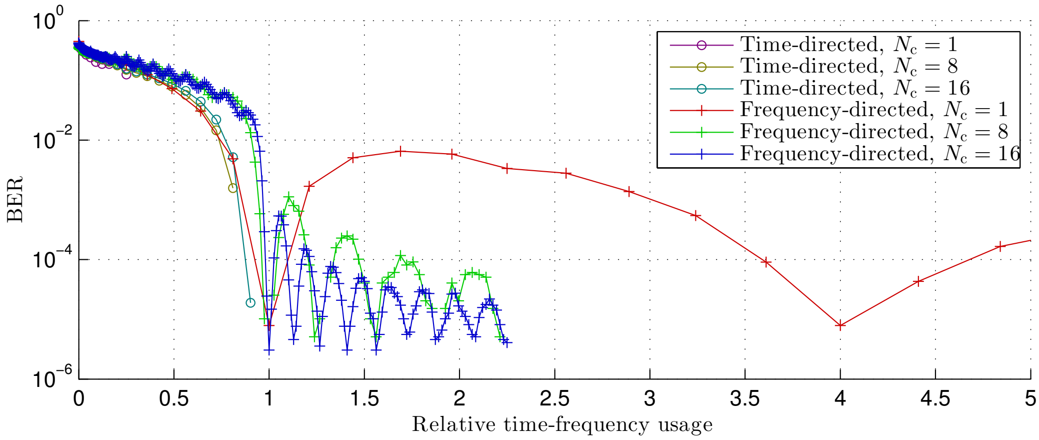

Figure 5.7: *Simulated BER of an OFDM system as a function of time-frequency usage. ISI occurs in one direction. Separate curves are shown for time- or frequency-directed ISI.* $E_b/N_0 = 10dB$.

extracted from the simulation results. Clearly, a single-subcarrier system requires a higher E_b/N_0 to meet the criterion than the systems with eight or sixteen subcarriers. Of the latter, the sixteen-subcarriers system has the smallest demand for additional E_b/N_0. If the additionally required E_b/N_0 is limited to 3dB, the achievable relative time-frequency usage is 1.3 for a single subcarrier, but 1.1 for eight or sixteen subcarriers. However, the plots in Figure 5.6 show that when the criterion is tightened to e.g. BER $\leq 10^{-4}$, a system with eight subcarriers demands a significantly higher E_b/N_0 and also the sixteen-subcarriers system requires a higher value.

The results suggest that adding subcarriers increases time-frequency efficiency of the Hermite system in AWGN channels. Because Hermite functions are orthogonal, there is no ICI in the system. The ISI is because of non-orthogonality between time-frequency-shifted Hermites. Hence, adding subcarriers means that non-orthogonal information bearers (symbols) are traded for orthogonal information bearers (subcarriers), reducing interference.

5.4 OFDM ISI

Many research publications have been focussing on missynchronization between the transmitter and receiver (single pair) of OFDM systems. Because multi-user communication is of interest here, every transmitter-receiver pair is assumed to be perfectly synchronized. However, missynchronization occurs between different pairs, giving rise to MAI [34].

In an OFDM system, the ISI that occurs when different transmitters are not synchronized, varies differently with symbol density than in a Hermite-based system.

Simulation results for time- and frequency-directed ISI are shown in Figure 5.7. To obtain clearer results, channel noise is added with $E_b/N_0 = 10$dB. Obviously, there is a difference between the two ISI directions. In the time direction, there is no ISI when $\zeta > 1$, because symbols do not overlap: an advantage of the strictly time-limitedness. However, in frequency direction, ISI is only absent when all subcarriers of all symbols together form an orthogonal set. These points are visible in Figure 5.7 as the (sharp) local minima of the BER curves.

For a multi-user case with successive symbols of different users, overlap may occur in the time direction. The plot shows that in this case, BER will increase steeply. This situation therefore benefits from a guard space between successive symbols, which is achieved with greater symbol spacing. The guard space can absorb a timing mismatch equal to its own duration, without any detrimental effects on received signal quality. However, throughput is reduced by the increased spacing.

For many subcarriers in an OFDM symbol, the average bandwidth per subcarrier is $1/T_{sym}$ (excluding sidelobes). A complete symbol occupies a bandwidth of N_c/T_{sym}. Hence, the time-frequency area per symbol is N_c, corresponding to the ideal spectral efficiency of two degrees of freedom per sHz.

For multiple frequency-shifted symbols, the condition to avoid ISI, when sidelobes are ignored, is

ζ	E_b/N_0 [dB]	
1.00	6.8	(+0.0)
1.21	11.3	(+4.5)
1.69	18.2	(+11.4)
1.96	15.8	(+9.0)
2.56	12.2	(+5.4)
2.89	10.7	(+3.9)
3.61	7.9	(+1.1)
4.00	6.8	(+0.0)

(a) *One subcarrier*

ζ	E_b/N_0 [dB]	
1.00	6.8	(+0.0)
1.03	7.4	(+0.6)
1.08	9.6	(+2.8)
1.10	10.2	(+3.4)
1.16	9.6	(+2.8)
1.18	8.6	(+1.8)
1.24	7.3	(+0.5)
1.27	6.8	(+0.0)

(b) *Eight subcarriers*

ζ	E_b/N_0 [dB]	
1.00	6.8	(+0.0)
1.01	7.2	(+0.4)
1.04	8.5	(+1.7)
1.05	9.0	(+2.2)
1.08	8.6	(+1.8)
1.09	8.1	(+1.3)
1.12	7.1	(+0.3)
1.13	6.8	(+0.0)

(c) *Sixteen subcarriers*

Table 5.5: *Minimum required E_b/N_0 to achieve BER $\leq 10^{-3}$ with OFDM-based transmission in an AWGN channel. Theoretically required value is 6.8dB without interference. The values between parentheses indicate the required additional E_b/N_0.*

that each symbol is at least shifted by N_c/T_{sym} (center-to-center distance) w.r.t. every other symbol. If sidelobes are taken into consideration, the center-to-center distance between every pair of symbols must be *exactly* $(N_c + n)/T_{sym}$ where n is any non-negative integer. This condition is enforced for OFDM/OFDMA. In the rectangular grid, this corresponds to $\zeta = (1 + n/N_c)^2$. These points are the local minima of the BER curves in Figure 5.7.

It can be seen in the figure, that the BER rises steeply for deviations from the ideal points. This can cause problems when multiple, unsynchronized users are transmitting. With regard to this case, Hermite-based communication allows the symbols to be placed at a slightly larger spacing, to reduce BER, because of the monotonically decreasing BER. For OFDM/OFDMA systems, however, a slightly larger spacing causes BER to increase. The next ideal point, which may tolerate (slightly) more deviation, requires a larger leap in spacing, causing spectral efficiency to jump down as well.

As the number of subcarriers increases, the jumps in relative time-frequency usage between the ideal points become smaller. This is because the bandwidth of a single subcarrier compared to total bandwidth is smaller when more subcarriers are employed. When viewed in the frequency domain only, the spacing between successive ideal points can be seen to equal the bandwidth of one subcarrier.

Figure 5.8 shows BER as a function of E_b/N_0 for an OFDM system that experiences frequency-directed ISI. When ISI occurs, its effect is similar for Hermite and OFDM systems: the BER approaches a lower-bound as E_b/N_0 increases. Table 5.5 lists the minimum required E_b/N_0 for the OFDM systems to meet the criterion of BER $\leq 10^{-3}$ for various values of ζ. Naturally, more ISI leads to a higher requirement on E_b/N_0 to meet the criterion. The shape of the frequency-directed results in Figure 5.7 returns in these values: highest E_b/N_0 is required when symbol spacing corresponds to the peaks of the curves.

Worst-case interference occurs when a single-carrier system is used with $\zeta \approx 1.69$. The requirement on E_b/N_0 then becomes 18.2dB. Should this situation occur, then a BER of e.g. 10^{-4} is not obtainable and a quite severe change in symbol spacing is required ($\zeta \approx 1.21$ or $\zeta \approx 2.56$ for the simulated step size) if this BER is necessary. For eight and sixteen subcarriers, the worst-case E_b/N_0 requirement is about 10.2dB and 9.0dB, respectively. However, the latter systems are still able to meet BER $\leq 10^{-4}$ if necessary, although a significantly higher E_b/N_0 is needed.

Adding subcarriers leads to a smaller performance penalty, in both BER and spectral efficiency, when missynchronization occurs (carrier frequencies are not in the ideal points). The same observation was done for the Hermite-based system, which was explained by the exchange of non-orthogonal for orthogonal information bearers.

5.5 Fourier-Hermite basis

Simulations of a Fourier-Hermite-based system yield the results shown in Figure 5.9. It can be seen that this system performs even better (for multiple subcarriers) than the normal Hermite system, because the BER is about two orders of magnitude lower when little noise is present. BER performance also improves faster with increased symbol spacing. The values for ζ_p of Table 5.6 show that

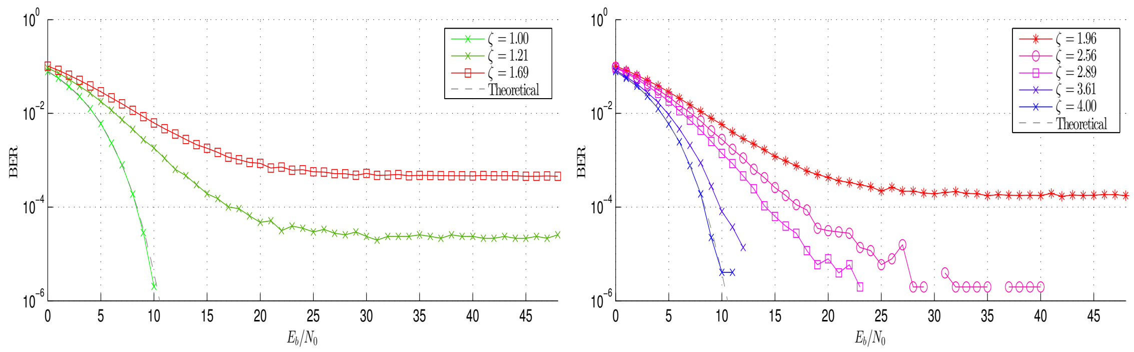

(a) *One subcarrier*

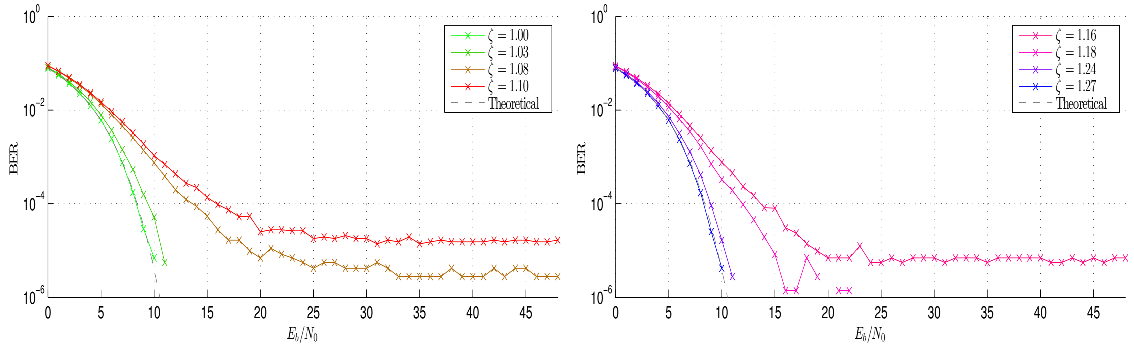

(b) *Eight subcarriers*

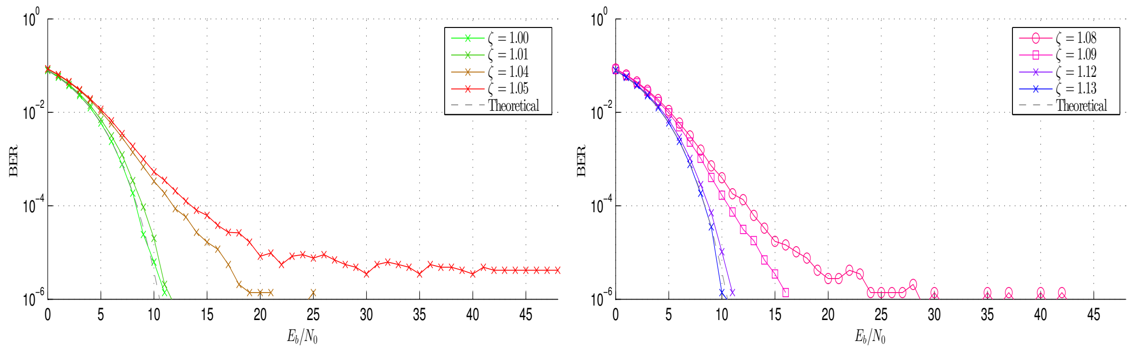

(c) *Sixteen subcarriers*

Figure 5.8: *Simulated noise influence on OFDM system's BER performance for various symbol densities in rectangular grid. Frequency-directed ISI only, with time-frequency usage corresponding to Equation 3.35. The chosen symbol densities are all in the range of the first sidelobe occurring in Figure 5.7.*

N_c	**Time-directed**	**Frequency-directed**	**Rectangular**	**Hexagonal**	
				Normal	Transposed
6	0.99	0.95		0.97	0.97
8	1.00	1.03	1.06	0.97	
16	1.08	1.08	1.10	0.97	

Table 5.6: *Pivotal time-frequency usage (ζ_p) of Fourier-Hermite system with various time-frequency symbol distributions. Values < 1 can occur because coding is excluded.*

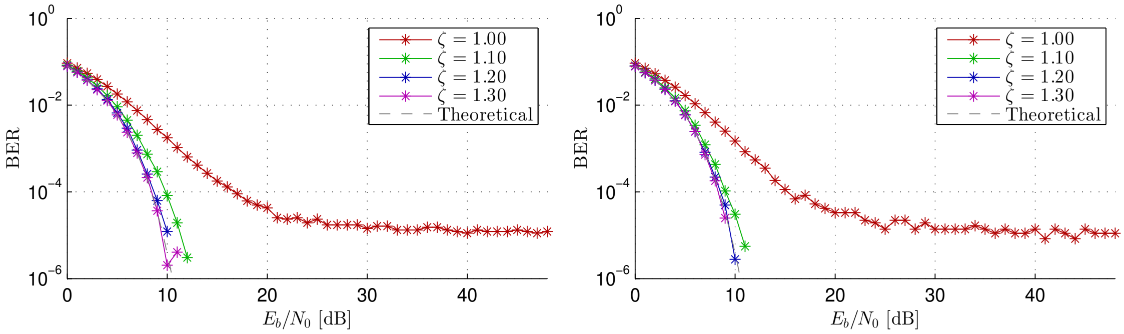

(a) *Eight subcarriers* **(b)** *Sixteen subcarriers*

Figure 5.9: *Simulated noise influence on Fourier-Hermite system's BER performance for various symbol densities in hexagonal grid.*

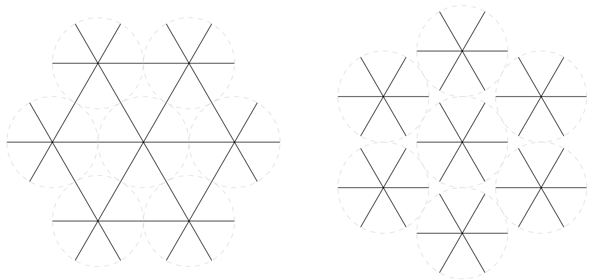

Figure 5.10: *Time-frequency illustrations of Fourier-Hermite symbols with six subcarriers in normal (left) and transposed (right) hexagonal grid.*

approximately optimal spectral efficiency is obtained with the Fourier-Hermite basis for the given BER limit of 10^{-3}. Note that the efficiency is reduced when coding is applied, which is necessary to reduce the final BER to zero.

Also, with the given BER criterion, a relative time-frequency usage of 1.1 requires for eight and sixteen subcarriers only 1.0dB and 0.4dB of extra E_b/N_0 (compared to interference-free theory), respectively, see Table 5.7. The Hermite system requires in these situations 2.3dB and 1.2dB.

An interesting situation occurs when six subcarriers are employed in the Fourier-Hermite system and a hexagonal symbol distribution is used, because of the flower-like pattern in time-frequency. In this situation, the hexagonal grid as described in section 2.10 causes the subcarriers of each symbol to point at the centers of the adjacent symbols. In a transposed version of the grid, the subcarriers point exactly between two adjacent symbols. This is illustrated in Figure 5.10. It is interesting to test whether the orientation of the grid influences performance for this system. Therefore, both distributions were simulated in order to compare total BER performances. The resulting pivotal time-frequency usages, listed in Table 5.6, do not show significant differences, suggesting that on average, the effect of interference is equal.

	E_b/N_0 [dB]			
ζ	$N_c = 8$		$N_c = 16$	
1.0	11.2	(+4.4)	10.8	(+4.0)
1.1	7.8	(+1.0)	7.2	(+0.4)
1.2	6.9	(+0.1)	6.8	(+0.0)
1.3	6.8	(+0.0)	6.8	(+0.0)

Table 5.7: *Minimum required E_b/N_0 to achieve BER $\leq 10^{-3}$ with Fourier-Hermite transmission in an AWGN channel. Theoretically required value is 6.8dB without interference. The values between parentheses indicate the required additional E_b/N_0.*

In this chapter, a variety of simulation and measurement results were presented. The effect of non-orthogonality between time-frequency-shifted Hermites on the BER of a Hermite-based communication system was examined by simulation and by transmission through a real channel. For the Hermite basis signals, BER decreases monotonically when symbol spacing in time-frequency is increased and for a given number of subcarriers, the higher orders are impaired more by the occurring ISI. The direction in the time-frequency plane in which ISI occurs is generally not of significant influence. However, some anomalies were observed for a single-subcarrier system when ISI occurs in a single direction. The exact cause for this deviant behavior has not become clear. In general, results from simulations and real-channel measurements agree very well, which was expected because the hardware was set up such, that the channel behaves predominantly like an AWGN channel.

When BER is restricted to 10^{-3}, a spectral efficiency of 1.85 degrees of freedom per sHz is shown to be possible with the Hermite system. In this case, the symbols are arranged in time-frequency according to a hexagonal grid and performance is strongly interference-limited. A rectangular grid performs slightly worse, with a spectral efficiency of around 1.7 degrees of freedom per sHz. These numbers do not include error-correction coding, which will reduce efficiency to achieve a BER of zero.

In many cases, the ISI is observed as a lower-bound on the BER when channel noise is reduced, i.e. interference-limited performance regimes are entered. In general, when compared to an interference-free system, a larger E_b/N_0 is required to compensate for the interference if BER is constrained. However, as subcarriers are added to the system, the demand for lower noise loosens, as orthogonality of the subcarriers within one symbol reduces interference. For a constraint BER $\leq 10^{-3}$ and with $E_\mathrm{b}/N_0 \geq$ 9.4dB (2.6dB more than interference-free systems), spectral efficiency is about 1.54 modulation degrees of freedom per second-Hertz for a single-subcarrier system and about 1.82 for eight and sixteen subcarriers, with the latter slightly less sensitive to a lower E_b/N_0. Again with a hexagonal time-frequency symbol grid.

A comparison of interference in the Hermite system and a (traditional) OFDM system was provided in this chapter. The effects of interference in case of multi-user missynchronization on the BER as a function of E_b/N_0 are similar for both systems: lower-bounds on BER for decreasing noise power and a requirement for higher E_b/N_0 to achieve the same BER. Most important difference between the systems in case of missynchronization between transmitters is that the Hermite system's BER monotonically decreases if symbols move away from each other, while the OFDM/OFDMA system's BER increases first. This allows a slightly increased symbol spacing to absorb the mismatch in a Hermite system. For the OFDM-based system, only discrete spacing increments give some improvement, but sensitivity to missynchronization remains, although slightly less severe with every next increment. For both systems, the total BER reduces when (orthogonal) subcarriers are added.

As a final addition to the investigations, a system employing the Fourier-Hermite basis signal set was examined briefly. The Fourier-Hermite system shares the pure-Hermite system's property of monotonically decreasing BER with increasing symbol spacing. As indicated earlier, this allows a slight reduction of efficiency in exchange for an improved BER and reduced sensitivity to missynchronization between users. Simulations have shown that performance of this system is superior to the pure Hermite system regarding achievable spectral efficiency and required E_b/N_0 for the used BER criterion. A spectral efficiency of about 1.82 modulation degrees of freedom per second-Hertz is achieved while requiring an E_b/N_0 of 7.8dB for eight subcarriers and 7.2dB for sixteen, which is 1.3dB and 0.8dB less than the comparable Hermite system and 1.0dB and 0.4dB above interference-free theory. For $E_\mathrm{b}/N_0 \geq$ 10.8dB (4.0dB more than interference-free), the spectral efficiency reaches 2 degrees of modulation freedom per second-Hertz, which is also the theoretical limit.

Chapter 6

Conclusions

The main aim of this thesis was to investigate the capabilities of Hermite basis signals in multi-carrier communication. The capabilities that were examined regard to spectral efficiency and unsychronized multi-user situations.

An important goal that was set at the start of this thesis, was to conduct real-world experiments with Hermite-based communication in order to verify theoretical and simulated performance. Aiming at this goal, we presented a setup that was employed in Hermite-based wireless transmission. This is the first time known to the author, in which actual data transmission through the air has been performed by using Hermite basis signals. It was observed for the Hermite-based system, that simulations and real-channel transmissions give very similar results. Thereby theoretical performance was verified with actual measurements.

The main research question for the thesis was: "How dense can the symbols of a Hermite-based communication system be packed in time-frequency, when the BER is constrained?" Based on existing literature about the capacity of error-correction coding schemes, the criterion BER $\leq 10^{-3}$ has been used. For this constraint, simulations have shown that the achievable density is about 0.06 symbols/s/Hz, for sixteen QPSK-modulated subcarriers in an AWGN channel with $E_b/N_0 \approx 46$dB. This corresponds to a spectral efficiency of approximately 1.89 modulation degrees of freedom per sHz. The symbols were arranged in time-frequency according to a hexagonal grid, which yields optimal density for symbols with a circular time-frequency representation, like the Hermites. Simulations of the same system employing a rectangular grid resulted in about 0.05 symbols/s/Hz, corresponding to about 1.67 degrees of freedom per sHz. Another set of basis signals derived from Hermite functions is the set of Fourier-Hermite signals, that were examined in this thesis as well. Simulation results have shown that this basis performs even better than a 'pure' Hermite function set. The theoretical limit of 2 degrees of modulation freedom per second-Hertz can be obtained with this basis when a hexagonal symbol grid is used and channel noise (AWGN) is about 4dB lower than for systems optimized for operation in AWGN.

The main research question was accompanied by the question: "How well is its spectral efficiency compared to e.g. OFDM?" Under the same circumstances, an OFDM system with a rectangular symbol grid (optimal for the OFDM symbol shape in time-frequency) can achieve the theoretical limit of 2 degrees of freedom per sHz. The results suggest that an OFDM system is superior regarding spectral efficiency. However, some implicit assumptions limit the significance of the numbers. The first is the assumption that there is one transmitter-receiver pair and both are perfectly synchronized in time and frequency. It is known that performance degrades when missynchronization between transmitter and receiver occurs and that OFDM is very sensitive in this respect. Secondly, it was assumed that this was the only system in a large available bandwidth and that it transferred a very large number of symbols. Hence, spectral leakage was neglected, but this is where a large difference lies: OFDM shows a slowly decaying ($\propto 1/\omega$) series of sidelobes in the frequency domain, whereas Hermites are known to be well-localized with exponential decay in both domains. Rapid decay is of importance for application in CR systems with regard to the use of white spaces without interfering neighboring transmitters.

Another point of interest at the start of this thesis considered spectrum-scarce, multi-user communication by the statement that it would be "interesting to know, how tolerant the [Hermite] system is to missynchronization between different transmitters and how this compares to OFDM/OFDMA." In this thesis, no elaborate quantitative investigation of missynchronization between transmitters was done. However, an indication of the tolerance is found by observing the change in BER when symbol density is varied. For the Hermite-based systems, it was found that the relation between symbol density and BER behaves monotonically: an increased density causes increased interference and BER, while a lower density causes less interference and lower BER. For OFDM/OFDMA, the relation is not monotonic in the frequency domain. It exhibits the "bouncing" pattern that is characteristic to the magnitude of a sinc-function, with sharp notches at the points where all carriers form an orthogonal set. Because normally an OFDMA system will be set to operate exactly in a notch of the BER curve, any deviation causes increased interference and BER. However, in the time domain, only for symbol densities that cause the time-limited symbols to overlap, interference occurs. In this situation, it decreases monotonically for increasing symbol distance.

The monotonic relation between symbol density and interference gives the opportunity to add a kind of guard space of arbitrary width between symbols, that can absorb mismatches in timing or frequency. The guard space is applicable to the Hermite system in both domains, but to the OFDM/OFDMA system only in the time domain. This is an advantage of the Hermite-based system in the unsynchronized multi-user case. The traditional solution to avoid interference by a large frequency spacing between (unsynchronized) transmitters is also a guard space, but it is required to be significantly wider than the possible mismatches, greatly degrading spectral efficiency.

In short, the communication systems based on Hermite functions show very promising performance with regard to spectral efficiency and unsynchronized multi-user situations. At the same time, they inherently keep out-of-band emission extremely low, which makes them good neighbors when residing in spectral white spaces.

6.1 Future work

Despite the work already performed, open questions remain and new questions are risen — in correspondence with scientific tradition.

Regarding the real-channel measurements, the close spacing of the transceiver antennas has resulted in a strong LOS path for the electro-magnetic waves to travel. In comparison to this, received power of reflections from IOs is justifiably negligible. As multi-path effects are not negligible in many realistic mobile channels, future research should include performance examination in more system-challenging setups.

An elaborate analysis of the effects caused by the missynchronization between multiple transmitters was not performed. Because the advantages of Hermite-based communication are expected to be fully appreciable in the unsynchronized multi-user case, future research in this direction is recommended.

The current investigation assumed perfect synchronization between transmitter and receiver. In practice, this synchronization is not perfect, inducing both ISI and ICI. It is recommended to look into the exact effects of transmitter-receiver missynchronization and the suitability of existing or even novel synchronization techniques.

By oversampling, the time-continuous behavior of the system was approximated. For practical implementation, e.g. energy efficiency will be important and thus the sample rate should be kept as low as possible. Conventional OFDM is capable of critical sampling, but because the spectral content of Hermite functions is significantly different, the lowest possible sampling rate is not determined in the same straightforward way. Therefore, it is recommended to investigate the effects of lower sampling rates on communication performance.

For pre- and post-processing of the signals, Matlab provides floating-point numerical precision. To reduce computational complexity, which is important for practical applications, fixed-point representations are preferred. As in any signal processing task, the loss of precision causes distortion of the signals, degrading system performance. Techniques exist to analyze processing chains in order to find the minimum numerical precision of variables in the system. If a practical implementation of a Hermite-based communication system is sought, it becomes necessary to investigate and minimize the effects of limited precision.

Our simulations and measurements were performed with symbols of equal size and shape. In a situation of multiple users, it is likely that each user prefers a different symbol rate and number of subcarriers. Therefore another direction for future research is adding diversity to these parameters and assessing the consequences to system performance. The regular grids that were proposed as time-frequency symbol distributions, will surely no longer suffice. Reduced regularity in the symbol distribution will lead to more degrees of freedom for optimization, creating a far more complex problem to solve.

Appendix A

List of acronyms

E_b/N_0	signal-to-noise ratio per bit
ACF	auto-correlation function
ADC	analog-to-digital converter
AM	amplitude modulation
AWGN	additive white Gaussian noise
BER	bit-error ratio
BPSK	binary phase shift keying
CAES	Computer Architecture for Embedded Systems
CCF	cross-correlation function
CP	cyclic prefix
CR	cognitive radio
DAB	Digital Audio Broadcast
DAC	digital-to-analog converter
DC	direct current
DFT	discrete Fourier transform
DSA	dynamic spectrum access
DSL	Digital Subscriber Line
DSP	digital signal processor/processing
FCC	Federal Communications Commission
FDM	frequency-division multiplexing
FDMA	frequency-division multiple access
FFT	fast Fourier transform
FM	frequency modulation
FPGA	field-programmable gate array
FrFT	fractional Fourier transform
GSM	Global System for Mobile Communications
ICI	inter-carrier interference
IF	intermediate frequency
IO	interacting object
ISI	inter-symbol interference
ISM	industrial, scientific and medical
LAN	local area network
LO	local oscillator
LOS	line of sight
MAI	multiple-access interference
MIMO	multiple input, multiple output
OFDM	orthogonal frequency-division multiplexing
OFDMA	orthogonal frequency division multiple access
PC	personal computer
PDF	probability density function

PSD	power spectral density
PSK	phase shift keying
PU	primary user
QAM	quadrature amplitude modulation
QPSK	quadrature phase shift keying
RF	radio frequency
RFID	RF Identification
S/N+D	signal-to-noise and distortion ratio
SDR	software defined radio
SIR	signal-to-interference ratio
SNR	signal-to-noise ratio
SSB	single sideband
SSBSC	single sideband supressed carrier
STFT	short-time Fourier transform
SU	secondary user
TBWP	time-bandwidth product
THD	total harmonic distortion
UHD	USRP Hardware Driver
USB	Universal Serial Bus
USRP	Universal Software Radio Peripheral
WLAN	wireless LAN

Bibliography

[1] Agilent Technologies. Spectrum Analysis Basics (Application Note 150), 2014.

[2] Ian F Akyildiz, Won-Yeol Lee, Mehmet C Vuran, and Shantidev Mohanty. NeXt generation/dynamic spectrum access/cognitive radio wireless networks: A survey. *Computer Networks*, 50(13):2127–2159, September 2006.

[3] L B Almeida. The fractional Fourier transform and time-frequency representations. *IEEE Transactions on Signal Processing*, 42(11):3084–3091, 1994.

[4] Analog Devices. AD9860/AD9862 Mixed-Signal Front-End (MxFE) Processor for Broadband Communications, 2002. datasheet.

[5] Jørgen Bach Andersen, Theodore S Rappaport, and Susumu Yoshida. Propagation measurements and models for wireless communications channels. *IEEE Communications Magazine*, (January):42–49, 1995.

[6] François Auger, Patrick Flandrin, Paulo Gonçalvès, and Olivier Lemoine. Time-Frequency Toolbox - For use with MATLAB. http://tftb.nongnu.org/, 1996.

[7] R J Beerends, H G Ter Morsche, J C Van den Berg, and E M Van de Vrie. *Fourier and Laplace Transforms*. 2003.

[8] Michael Buettner and David Wetherall. A software radio-based UHF RFID reader for PHY/MAC experimentation. *2011 IEEE International Conference on RFID*, pages 134–141, April 2011.

[9] Wachira Chongburee, Timothy Pratt, and Dennis G Sweeney. *Digital Transmission by Hermite N-dimensional Antipodal Scheme*. PhD thesis, 2004.

[10] Johann Cigler. Continuous q-Hermite polynomials: An elementary approach. *arXiv preprint arXiv:1307.0357*, pages 1–31, 2013.

[11] Leonard J Jr Cimini. Analysis and simulation of a digital mobile channel using orthogonal frequency division multiplexing. *IEEE Transactions on Communications*, 33(7):665–675, 1985.

[12] Leon Cohen. Time-frequency distributions-a review. *Proceedings of the IEEE*, 77(7), 1989.

[13] Ettus Research. Ettus Research. http://www.ettus.com.

[14] Ettus Research. Schematic USRP2. http://files.ettus.com/schematics/usrp2/usrp2.pdf, 2012.

[15] Ettus Research. Schematic WBX. http://files.ettus.com/schematics/wbx/wbx.pdf, 2012.

[16] Harald T Friis. A note on a simple transmission formula. *Proceedings of the I.R.E. and Waves and Electrons*, (1):254–256, 1946.

[17] Lenny Fukshansky. Revisiting the hexagonal lattice: on optimal lattice circle packing. *arXiv preprint arXiv:0911.4106*, pages 1–8, 2009.

[18] GNU Radio. GNU Radio. http://www.gnuradio.org.

[19] Vinoth Gunasekaran and Fotios C Harmantzis. Emerging wireless technologies for developing countries. *Technology in Society*, 29(1):23–42, January 2007.

[20] Ralf Haas and Jean-Claude Belfiore. A time-frequency well-localized pulse for multiple carrier transmission. *Wireless Personal Communications*, 5(1):1–18, 1997.

[21] IEEE LAN/MAN standards Committee. Part 11: Wireless LAN medium access control (MAC) and physical layer (PHY) specifications. *IEEE-SA Standards Board*, 2012.

[22] Karlsruhe Institute of Technology. Simulink-USRP: Universal Software Radio Peripheral (USRP) Blockset. http://www.cel.kit.edu/english/usrp.php.

[23] Cornelis Willem Korevaar. A Time-Frequency Localized Signal Basis for Multi-Carrier Communication. Master's thesis, University of Twente, The Netherlands, June 2010.

[24] Cornelis Willem Korevaar, André B J Kokkeler, Pieter-Tjerk de Boer, and Gerard J M Smit. Synchronization and matched filtering in time-frequency using the sunflower spiral. *2012 IEEE Global Communications Conference (GLOBECOM)*, (1):3959–3964, December 2012.

[25] Cornelis Willem Korevaar, André B J Kokkeler, Pieter-Tjerk de Boer, and Gerard J M Smit. Fourier-Hermite Communications; Where Fourier Meets Hermite. *IEEE International Conference on Acoustics, Speech and Signal Processing (ICASSP)*, pages 4723–4727, 2013.

[26] Cornelis Willem Korevaar, Mark Stefan Oude Alink, Pieter-Tjerk de Boer, André B J Kokkeler, and Gerard J M Smit. Closed-form Expressions for Time-Frequency Operations involving Hermite Functions. *IEEE Transactions on Signal Processing (Submitted for review)*.

[27] Werner Kozek and Andreas F Molisch. Nonorthogonal pulseshapes for multicarrier communications in doubly dispersive channels. *IEEE Journal on Selected Areas in Communications*, 16(8):1579–1589, 1998.

[28] H J Landau and H O Pollak. Prolate Spheroidal Wave Functions, Fourier Analysis and Uncertainty II. *Bell System Technical Journal*, 40(1):65–84, 1961.

[29] Upamanyu Madhow. *Fundamentals of digital communication*. 2008.

[30] JB Martens. The Hermite transform-theory. *IEEE Transactions on Acoustics, Speech, and Signal Processing*, 38(9):1595–1606, 1990.

[31] David Mendlovic and Haldun M Ozaktas. Fractional Fourier transforms and their optical implementation: I. *Journal of the Optical Society of America A*, 10(9):1875–1881, December 1993.

[32] Andreas F Molisch. *Wireless Communications*. John Wiley & Sons Ltd., first edition, 2005.

[33] Andreas F Molisch. *Wireless Communications*. second edition, 2011.

[34] Michele Morelli, C.-C. Jay Kuo, and Man-On Pun. Synchronization Techniques for Orthogonal Frequency Division Multiple Access (OFDMA): A Tutorial Review. *Proceedings of the IEEE*, 95(7):1394–1427, July 2007.

[35] OpenBTS. OpenBTS. http://www.openbts.org.

[36] Opendigitalradio.org. Opendigitalradio.org. http://www.opendigitalradio.org.

[37] Mark Stefan Oude Alink. *RF spectrum sensing in CMOS exploiting crosscorrelation*. PhD thesis, University of Twente, 2013.

[38] Thierry Pollet, Mark Van Bladel, and Marc Moeneclaey. BER sensitivity of OFDM systems to carrier frequency offset and Wiener phase noise. *IEEE Transactions on Communications*, 43(2/3/4):191–193, 1995.

[39] John G Proakis. *Digital communications*.

[40] Marguerite Reardon. FCC chairman pushes policy agenda, January 2010. http://www.cnet.com/8301-31045_1-10430991-269.html.

[41] Claude E Shannon. A Mathematical Theory of Communication. *Bell System Technical Journal*, 27(July 1948):379–423, 1948.

[42] Bernard Sklar. Rayleigh Fading Channels in Mobile Digital Communication Systems Part I: Characterization. *IEEE Communications Magazine*, (July):90–100, 1997.

[43] Lodewijk T Smit. *Energy-efficient wireless communication*. PhD thesis, University of Twente, 2004.

[44] The MathWorks. USRP Support Package from Communications System Toolbox. http://www.mathworks.com/hardware-support/usrp.html.

[45] MR Walton and H Hanrahan. Hermite wavelets for multicarrier data transmission. *1993 IEEE South African Symposium on Communications and Signal Processing*, pages 40–45, 1993.

[46] Alexander M Wyglinski, Di Pu, and Daniel J Cullen. Digital communication systems education via software-defined radio experimentation. In *Proceedings of the 118th ASEE Annual Conference and Exposition*, pages 26–29, Vancouver, BC, Canada, 2011.